Petroleum Science 23 (2026) 7338–7354

Contents lists available at ScienceDirect

Petroleum Science

journal homepage: www.keaipublishing.com/en/journals/petroleum-science

Original Paper

Study on multiscale effects and mechanisms of induced organic precipitation on reservoir wettability during CO_2 huff-n-puff in shale oil reservoirs

Bo Han [a,b,c,d], Hui Gao [a,c,d,*], Zheng-Dong Lei [e], Kai-Qing Luo [a,c,d], Xiao-Hang Li [a,c,d], Guo-Qing Li [a,c,d], Zhi-Lin Cheng [a,c,d], Teng Li [a,c,d], Chen Wang [a,c,d]

[a] School of Petroleum Engineering, Xi'an Petroleum University, Xi'an, 710065, Shaanxi, China
[b] Faculty of Mining Engineering, Shanxi Institute of Energy, Taiyuan, 030600, Shanxi, China
[c] Key Laboratory of Exploration and Development of Complex and Difficult-to-Produce Oil & Gas Reservoirs (Xi'an Petroleum University), Ministry of Education, Xi'an, 710065, Shaanxi, China
[d] Xi'an Key Laboratory of Tight Oil (Shale Oil) Development, Xi'an, 710065, Shaanxi, China
[e] Research Institute of Petroleum Exploration and Development, PetroChina, Beijing, 100083, China

ARTICLE INFO

Article history:
Received 21 December 2025
Received in revised form
3 June 2026
Accepted 2 July 2026
Available online 9 July 2026

Edited by Meng-Jiao Zhou

Keywords:
Shale oil
CO_2 huff-n-puff
Organic precipitation
Wettability alteration
Characteristics and mechanisms of wettability alteration

ABSTRACT

During CO_2 injection in shale oil, CO_2–crude oil interactions promote the precipitation of heavy organic fractions, which in turn alters the reservoir wettability. In this work, CO_2 huff-n-puff tests were designed and performed in combination with contact angle measurements and one-/two-dimensional nuclear magnetic resonance (NMR) spectroscopy to investigate the multiscale effects of organic precipitation on reservoir wettability. A pore-scale water-wetness index was established using 1D NMR T_2 spectra to quantitatively characterize the microscopic wettability evolution across various pore-size ranges. The mechanisms underlying wettability alteration were elucidated by analyzing changes in crude oil composition, shale surface morphology, and pore structure before and after CO_2 exposure. Results indicate that the overall water-wetness of the reservoir is markedly weakened after CO_2 huff-n-puff. Both macroscopic and microscopic wettability alterations exhibit consistent trends, evolving from strongly water-wet toward intermediate-wet and ultimately weakly oil-wet states as injection pressure, temperature, and soaking duration increase. Across various pore-size ranges, the reduction in water-wetness follows the order: micropores > small pores > mesopores > macropores. Notably, changes in the wettability of small pores have the strongest impact on the overall core wettability. The alteration of reservoir wettability is mainly governed by the precipitation of heavy organic fractions, together with modifications in surface roughness and pore structure. Correlation analysis reveals strong relationships between the precipitation ratios of resins and asphaltenes and the contact angle, with corresponding correlation coefficients of 0.8284 and 0.9328, respectively, highlighting that asphaltene precipitation has a more pronounced impact on wettability alteration. Moreover, organic precipitation increases surface roughness and decreases pore space, further diminishing water-wetness. Strong correlations are observed between contact angle and core-surface roughness, as quantified by arithmetic mean roughness (Ra) and root-mean-square roughness (Rq), yielding correlation coefficients of 0.8942 and 0.9116, respectively. Meanwhile, the correlation coefficient between pore volume variation and the pore-scale water-wetness index reaches 0.9503, highlighting that pore structure alteration plays a vital role in wettability evolution. This study elucidates the multiscale mechanisms by which organic precipitation controls wettability alteration, offering fundamental insights into enhanced oil recovery and the secure long-term storage of CO_2 within shale formations.

© 2026 The Authors. Publishing services by Elsevier B.V. on behalf of KeAi Communications Co. Ltd. This is an open access article under the CC BY-NC-ND license (http://creativecommons.org/licenses/by-nc-nd/4.0/).

* Corresponding author.
E-mail address: ghtopsun1@163.com (H. Gao).
Peer review under the responsibility of China University of Petroleum (Beijing).

https://doi.org/10.1016/j.petsci.2026.07.003
1995-8226/© 2026 The Authors. Publishing services by Elsevier B.V. on behalf of KeAi Communications Co. Ltd. This is an open access article under the CC BY-NC-ND license (http://creativecommons.org/licenses/by-nc-nd/4.0/).

1. Introduction

Sustained global economic growth has driven a continual rise in energy demand, thereby increasing interest in unconventional hydrocarbon exploration, particularly shale oil. Shale oil has become a promising alternative to conventional petroleum due to its widespread availability and potential to enhance energy security. Abundant shale oil is present in China and is primarily concentrated within prominent continental sedimentary basins, including the Junggar, Ordos and Jianghan basins (Li et al., 2022; Liu et al., 2025b; Jin et al., 2021). China's geological shale oil resources are expected to be 39.746 billion tons. The medium-to high-maturity continental shale oil accounts for approximately 28.3 billion tons, highlighting its strategic importance as an alternative to conventional petroleum (Jia et al., 2024). In 2024, onshore shale oil production in China surpassed four million tons, making a notable contribution to the growth of the country's crude oil output (Gao et al., 2025).

However, shale oil reservoirs exhibit complex pore structures, dominated by micro- and nanopores, along with strong heterogeneity, high organic matter content, and diverse mineral compositions (Han et al., 2021, 2025; Mănescu and Nuno, 2015; Xu et al., 2022). These geological features lead to poor oil mobility and low single-well productivity. In addition, owing to the clay-rich nature of shale formations, conventional water-flooding techniques are poorly suited to shale reservoirs. Currently, shale oil exploitation mainly depends on horizontal wells combined with large-scale hydraulic fracturing, followed by depletion production (Na et al., 2012; Yuan et al., 2023a; Zhao et al., 2023; Bao et al., 2023). Due to lack of energy replenishment, reservoir pressure declines rapidly, resulting in a sharp drop of oil production. The estimated primary recovery factor for shale oil is only about 5%–10%, which is much lower than that of conventional reservoirs (Yuan et al., 2023b; Zhu et al., 2023; Yun et al., 2023).

CO_2-based EOR has emerged as an attractive option for enhancing recovery efficiency in shale oil (Li et al., 2023a, 2023b; Cao and Gu, 2013). Owing to its unique physicochemical properties such as low miscibility pressure, high diffusivity in crude oil, significant viscosity reduction and interfacial tension reduction, CO_2 can effectively mobilize oil stored in micro- and nanopores (Li et al., 2024; Zou et al., 2022). Both laboratory- and field-scale studies have been conducted in formations such as the Bakken shales in North America, as well as the Chang 7 Member of the Ordos Basin and the Gulong Depression in the Songliao Basin (Dong et al., 2023; Huang et al., 2023a). Results demonstrate that CO_2 readily dissolves in shale oil. The miscibility pressure between shale oil and CO_2 is relatively low, allowing substantial recovery enhancement under miscible conditions. Compared with other injected gases, CO_2 achieves superior recovery improvements, with huff-n-puff operations increasing recovery efficiency by 33%–85%. These advantages make CO_2-EOR a promising technology for shale oil reservoirs and a major focus of current research.

Nevertheless, CO_2 injection into shale formations induces complex physicochemical interactions with crude oil, leading to the precipitation of heavy organic fractions including asphaltenes and resins. These precipitates can modify pore structures and reservoir properties, thereby influencing oil mobilization efficiency (Tian et al., 2023). Previous studies have shown that asphaltene precipitation during CO_2–oil interactions can significantly reduce reservoir permeability and alter pore structures. For example, Lee et al. (2019) demonstrated through reservoir simulations that asphaltene precipitation during CO_2 injection reduces both porosity and permeability. Li et al. (2019) reported that CO_2 promotes the formation of larger asphaltene aggregates compared with CH_4 and N_2, particularly with increasing reaction time. Using NMR techniques, Qian et al. (2020) found that higher injection pressures intensify asphaltene precipitation and consequently impair reservoir permeability. Shen and Sheng (2018) further observed that repeated CO_2 injection in Wolfcamp shale cores reduced permeability by 48.5%, with asphaltenes mainly depositing near the injection end. Numerical simulations by Lee et al. (2020) also suggested that nano-confinement effects in shale nanopores may further enhance asphaltene precipitation during CO_2 injection.

In addition to modifying pore structures, asphaltene precipitation can also alter reservoir wettability. Wang et al. (2020) found that CO_2 injection promotes adsorption of asphaltenes on mineral surfaces, resulting in wettability alteration. Wei et al. (2020) reported that rising CO_2 pressure accelerates asphaltene precipitation, although the wettability change is mainly confined to the region near the core inlet. Wang et al. (2021) showed that CO_2-induced asphaltene precipitation weakens the water-wetness of shale cores, particularly in samples with relatively homogeneous pore structures, whereas miscible flooding can mitigate this effect. Huang et al. (2023b) further demonstrated that asphaltene deposition enhances surface oil-wetness and increases oil-phase flow resistance. More recently, Huang et al. (2024) confirmed that adsorbed asphaltenes significantly reduce the water-wetness of initially strongly hydrophilic rocks.

In addition to laboratory studies, CO_2 injection has been widely practiced in several shale oil basins in China, demonstrating considerable potential for enhanced oil recovery. For example, following the implementation of CO_2 injection, cumulative oil production from Well GY40 in Gulong shale increased nearly thirteenfold, reaching 463 t from an initial 36 t (Cheng et al., 2025). In the Ordos Basin, a simultaneous CO_2 huff-n-puff energy supplementation practice was conducted in five horizontal wells, with cumulative CO_2 injection volumes ranging from 1.2×10^4 t to 1.7×10^4 t per well. The formation pressure increased from 8.5 MPa to 21.4 MPa, and the peak liquid production rate reached 7.70–38.10 m^3/d (Niu et al., 2025). In the Subei basin, CO_2 was also engaged to enhance shale oil recovery. For well LY1-1, the cumulative incremental oil production was estimated at approximately 2500 t, corresponding to an oil exchange ratio of 0.25 t/t (Yao et al., 2026).

However, field applications have also revealed several technical challenges that may limit the effectiveness of CO_2 injection (Li et al., 2025). Interactions between injected CO_2 and crude oil can induce the precipitation of heavy organic components, which may lead to permeability reduction and formation damage, thereby compromising the long-term performance of CO_2-EOR operations (Ren et al., 2024). For instance, asphaltene deposition in the Yongjin Oilfield has resulted in recurrent wellbore blockages, increased operational costs, and significant production decline, even with repeated cleanout operations (Yang et al., 2025). In addition, the strong heterogeneity of shale reservoirs and the discrepancy between laboratory conditions and field-scale environments further complicate the prediction of reservoir responses during CO_2 injection (Liu et al., 2025a; Dong et al., 2020). Therefore, clarifying the physicochemical mechanisms governing CO_2–oil interactions and the associated wettability evolution during CO_2–oil–shale reactions is vital for supporting the optimization of CO_2 injection schemes and facilitating the safe, efficient deployment of CO_2-EOR and long-term geological CO_2 storage.

In summary, existing studies have shown that heavy organic fractions, such as resins and asphaltenes, tend to precipitate during CO_2-based shale oil recovery, thereby altering reservoir physical properties, pore structures, and wettability, ultimately impacting oil recovery efficiency. However, most of these investigations have focused on static CO_2–oil interactions, while the

Table 1
The physical parameters of the cores.

Sample number	Length, mm	Diameter, mm	TOC, %	R_o, %	Porosity, %	Permeability, $\times10^{-3}$ μm^2
1	25.45	25.32	2.54	0.76	6.56	0.0393
2	25.68	25.31	2.48	0.79	7.02	0.0463
3	21.48	25.34	2.13	0.75	7.56	0.0577
4	25.84	25.31	2.34	0.93	8.01	0.0760
5	26.90	25.35	2.64	0.92	6.12	0.0228
6	25.35	25.32	2.12	0.95	6.33	0.0207
7	24.45	25.31	2.56	0.83	6.24	0.0181
8	26.67	25.31	2.33	0.76	7.10	0.0205
9	23.96	25.26	2.48	0.79	7.32	0.0528
10	26.61	25.31	2.45	0.82	7.65	0.0650
11	25.82	25.29	2.21	0.81	6.78	0.0185
CV (%)	6.12	0.09	7.40	8.73	8.96	52.88

dynamic processes involved in CO_2 injection and their effects on wettability evolution remain insufficiently explored. Furthermore, wettability characterization has primarily relied on macroscopic contact angle measurements, which capture surface-scale changes but do not reflect pore-scale wettability evolution.

In this study, shale oil core samples from the Ordos Basin were systematically analyzed to evaluate wettability evolution at both macroscopic and microscopic scales during CO_2 huff-n-puff. Contact angle tests, 1D T_2 spectra, and 2D T_1–T_2 spectra were integrated to capture wettability changes across multiple scales. By combining these results with analyses of crude oil composition, shale surface morphology, and pore structure variations, the mechanisms by which organic precipitation regulates reservoir wettability are elucidated. These findings provide theoretical guidance for improving shale oil recovery through CO_2 injection and contribute to the scientific evaluation of the security of geological CO_2 sequestration.

2. Experimental methods and principles

2.1. Materials and equipment

To examine how organic precipitates, including resins and asphaltenes, affect reservoir wettability during CO_2 injection, core samples were obtained from the Chang 7 Member of the Ordos Basin. Table 1 presents the physical properties of the cores. Quantitative mineral compositions were determined using X-ray diffraction (XRD), indicating that the samples mainly compose of clay minerals, quartz, and feldspar, with minor carbonate minerals (Table 2).

To evaluate sample homogeneity, the coefficient of variation (CV) of mineral composition and key petrophysical parameters was calculated. The CV values of clay mineral content are all below 5%, while those of TOC, porosity and other petrophysical parameters are all lower than 10%, indicating good consistency among the samples. Although the CV of permeability reaches 52.88%, which is mainly attributed to the extremely low permeability values of shale cores, which make the CV highly sensitive. The standard deviation of permeability is only 0.0210×10^{-3} μm^2, suggesting limited variability among samples. These results confirm that the selected cores exhibit acceptable mineralogical and petrophysical consistency for the experimental study.

For convenient core saturation, the oil engaged in the experiments was a mixture of degassed crude oil from the Chang 7 formation and kerosene at a volumetric ratio of 3:1. Under conditions of 20 °C and 0.1 MPa, the blended oil possessed a density of 0.78 g/cm^3 along with a viscosity of 2.0 mPa s.

The experimental setup primarily comprised a core flooding unit, a core holder assembly, a low-field NMR system, along with pressure monitoring and temperature control units (See Fig. 1). The core flooding unit was equipped with a 2 PB–104IV precision pump (Beijing Xingda Technology Development Co., Ltd., China), which operates at pressures of 0–40 MPa and provides flow rates of 0.001–10 mL/min. The core holder assembly utilized a core holder with a maximum operating pressure of 40 MPa. The low-field NMR setup consisted of a PQ001 spectrometer (Suzhou Niumag, China), enabling measurements with a magnetic field of 0.28 ± 0.03 T. The pressure monitoring unit incorporated multiple pressure sensors, while the temperature control unit employed electric heating jackets to ensure stable thermal conditions throughout the experiments.

2.2. Methods and procedures

To simulate the wettability alteration characteristics of shale oil reservoirs subjected to CO_2 under various experimental

Table 2
The mineral compositions of the cores.

Sample number	Content, %								
	Quartz	Feldspar	Calcite	Dolomite	Pyrite	Illite	I/S	Chlorite	Kaolinite
1	25.66	16.03	5.44	3.39	0.69	18.94	17.40	8.91	3.54
2	25.47	15.92	5.86	3.51	0.72	19.24	17.13	8.53	3.62
3	26.17	15.58	5.64	3.52	0.74	19.06	16.65	8.96	3.68
4	25.65	15.51	5.45	3.65	0.66	19.23	17.37	8.63	3.85
5	23.64	16.05	5.64	3.37	0.65	20.16	17.14	9.44	3.91
6	25.13	16.17	5.44	3.70	0.72	19.06	17.14	8.94	3.70
7	24.99	16.42	5.98	3.73	0.72	18.90	16.49	9.18	3.59
8	25.14	15.67	5.58	3.74	0.69	19.19	17.39	8.82	3.78
9	25.29	16.22	5.32	3.61	0.67	19.33	17.21	8.70	3.65
10	24.58	16.34	5.75	3.58	0.68	19.01	17.34	8.98	3.74
11	24.91	16.82	5.64	3.62	0.72	19.17	16.93	8.41	3.78
CV (%)	2.62	2.43	3.50	3.45	4.06	1.79	1.78	3.34	3.00

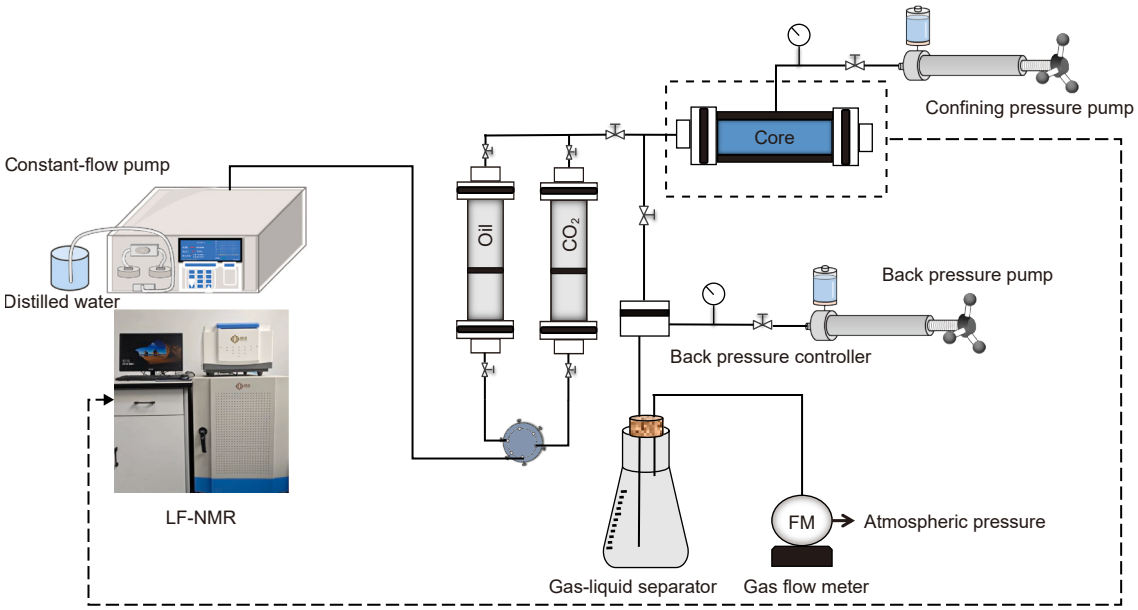


Fig. 1. Experimental schematic diagram of CO_2 huff-n-puff.

Table 3
Experimental categories and parameter design.

Sample number	Experimental categories	Pressure, MPa	Temperature, °C	Soaking durations, d	Notes
1	Pressure-controlled category	10	70	5	
2		15	70	5	
3		20	70	5	Cross group
4		25	70	5	
5	Temperature-controlled category	20	40	5	
6		20	50	5	
7		20	60	5	
8		20	80	5	
9	Soaking-time-controlled category	20	70	2	
10		20	70	10	
11		20	70	15	

conditions, three categories of experiments (pressure-controlled, temperature-controlled, and soaking-time-controlled categories) were conducted using eleven natural shale cores, as listed in Table 1. The Chang 7 reservoir is buried at depths of 1500–2500 m, with an average geothermal gradient of approximately 2.5 °C/100 m and a formation pressure coefficient of 0.85–1.10. Based on these in-situ conditions, the pressure-controlled experiments were performed at 10–25 MPa, the temperature-controlled experiments at 40–80 °C, and the soaking-time-controlled experiments with soaking durations of 2–15 days. The experimental categories and parameters are summarized in Table 3.

The precipitation of heavy organic fractions, including resins and asphaltenes can significantly alter reservoir wettability. In this work, CO_2 huff-n-puff tests were performed under various conditions. By combining macroscopic contact angle measurements with 1D T_2 and 2D T_1–T_2 spectra, the multiscale effects of organic precipitation on wettability were thoroughly assessed. Following procedures analogous to field CO_2 huff-n-puff operations, the experimental workflow was set as follows.

(1) Core preparation: All natural core samples were first screened and labeled for identification. The cores were then subjected to deep cleaning using a petroleum ether–benzene mixture (volume ratio 1:3) at 5 MPa and 80 °C for seven consecutive days. After cleaning, the cores were oven-dried at 90 °C for 48 h under controlled temperature conditions.

(2) Pre-experiment characterization: The dried cores were weighed, and their gas permeability, water wettability contact angle, and NMR T_2 and T_1–T_2 spectra were measured to characterize their initial physical properties.

(3) Water saturation and NMR tests: The cleaned and dried cores were saturated with water through spontaneous imbibition under ambient conditions and subsequent pressurized saturation at 25 MPa. NMR T_2 and T_1–T_2 spectra were acquired after each water saturation stage.

(4) Oil saturation: The cores were re-dried and subsequently saturated with simulated oil at a constant injection rate of 0.02 mL/min. Once a stable oil efflux was observed at the outlet, oil saturation was considered complete. Subsequently, the NMR T_2 and T_1–T_2 spectra of the cores were measured.

(5) CO_2 injection and soaking: CO_2 was introduced into the cores at a steady flow rate of 0.1 mL/min. When the pressure inside the core holder reached the predetermined experimental value, CO_2 injection was discontinued, with the inlet and outlet valves subsequently secured. The cores were then subjected to soak for the designated duration specified in the experimental design.

(6) Depressurization and oil recovery: After the soaking, the inlet valve was opened, and the core holder was depressurized gradually in a stepwise manner under back-pressure control. The oil produced during depressurization was collected and weighed. After depressurization, the cores were removed from the holder for subsequent NMR measurements.
(7) Oil composition and shale property analysis: Produced oil samples were analyzed to investigate the effects of CO_2 exposure on oil compositions. In addition, the shale surface morphology and pore structure were examined to assess variations induced by CO_2 exposure.
(8) Post-experiment characterization: Steps (1)–(3) were subsequently applied to the post-treated cores, encompassing oil cleaning, water contact angle measurements, and NMR analyses of dry, spontaneously water-saturated, and pressurized water-saturated cores.

In this study, a petroleum ether–benzene mixture was used to wash the core samples prior to wettability measurements. The solvent effectively removes residual movable oil and light hydrocarbons, minimizing their interference with wettability evaluation, while its limited ability to dissolve heavy fractions such as resins and asphaltenes allows the CO_2-induced precipitates to be largely preserved. This enables a more reliable assessment of the impact of resin and asphaltene precipitation on shale wettability.

As for the water contact angle, although the water–oil–rock contact angle is more representative of reservoir multiphase flow conditions, the water–air–rock contact angle is widely used as a proxy indicator to characterize relative wettability alteration due to its experimental simplicity and stability. The measurements in this study are therefore intended to evaluate the relative change in rock wettability induced by CO_2 exposure rather than to directly quantify in-situ capillary behavior.

2.3. NMR-based method for determining the pore-scale water-wetness index

Common methods for characterizing rock wettability, such as contact angle measurements, can quantify the macroscopic surface wettability of rocks, whereas the USBM and Amott index methods are widely employed to characterize the overall wettability of core samples. However, these traditional approaches are insufficient for effectively describing the microscopic wettability of pores at different scales within the core.

In this work, a new approach based on NMR measurements was proposed to determine pore-scale water wettability at the microscopic level. This approach establishes a core pore-scale water-wetness index (I_W) based on 1D NMR T_2 spectra of cores under different conditions: the dry, spontaneous water imbibition, and pressurized water-saturated states. The index provides a quantitative measure of the degree of water wettability across pore sizes of different scales. The core pore-scale water-wetness index (I_W) is defined as follows:

$$I_W = \frac{S_2 - S_1}{S_3 - S_1} \quad (1)$$

where S_1 represents integrated area of the T_2 spectrum obtained from the dry core, ms; S_2 represents the integrated area of the T_2 spectrum obtained from the core after spontaneous water imbibition, ms; S_3 represents integrated area of the T_2 spectrum obtained from the core after pressurized water saturation, ms.

As illustrated in Fig. 2, the procedure for establishing the core pore-scale water-wetness index (I_W) is as follows. The core

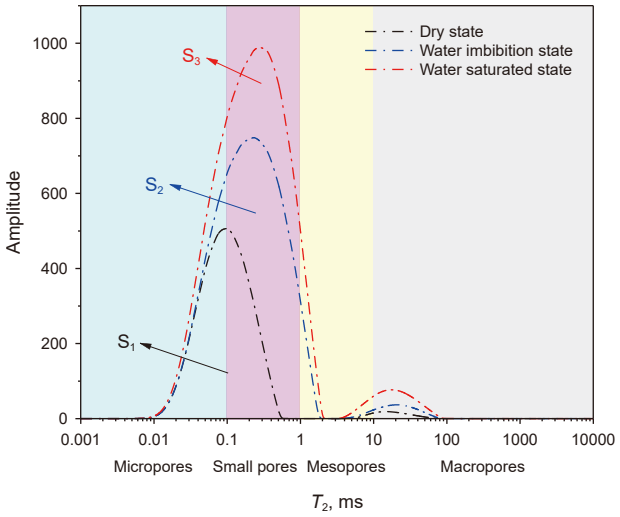


Fig. 2. Establishment process of the core pore-scale water-wetness index (I_W).

samples were initially oven-dried at 90 °C for 24 h to eliminate free water from both the surface and pore space. However, residual hydrogen signals were still detected in the dry state, attributable to organic matter, structurally bound water within minerals, and isolated (non-connected) pores. The integrated area of the NMR T_2 spectrum obtained from the dry core, denoted as S_1, represents the signal contribution from organic matter, mineral-bound water, and isolated pores.

Subsequently, the dried cores were subjected to spontaneous imbibition under ambient conditions (20 °C, 0.1 MPa) for 24 h. Driven by capillary forces, water spontaneously entered the hydrophilic pores of the cores. The NMR T_2 spectrum was then measured and integrated to obtain S_2, with the difference (S_2–S_1) representing the amount of water imbibed into the hydrophilic pores.

Following the imbibition stage, the cores were further subjected to pressurized water saturation at 25 MPa for 24 h. Under these high-pressure conditions, water was able to penetrate all effectively connected pores, including both hydrophilic and hydrophobic ones. The integrated area of the T_2 spectrum measured after pressurized water saturation, denoted as S_3, represents the total water volume occupying all connected pores, while the difference (S_3–S_1) corresponds to the overall accessible pore volume.

Therefore, the core pore-scale water-wetness index (I_W), as defined in Eq. (1), quantitatively describes the ease with which water invades the core's pore network, thereby characterizing its overall water-wetness. A higher I_W value indicates that water can more readily penetrate the pore system, reflecting stronger water-wet characteristics. When $I_W = 1$, the core is considered completely water-wet. Conversely, a lower I_W value indicates more restricted water penetration and weaker water-wetness. When $I_W = 0$, the core is regarded as completely oil-wet.

In this study, spontaneous imbibition experiments were performed in a water–air–rock system, where dry cores were immersed in brine and measured by NMR. Although this configuration differs from the water–oil–rock system in actual reservoirs, the air–phase imbibition approach is widely used as a proxy for wettability evaluation because it avoids the complexity of oil–water interactions and enables clearer interpretation of wettability alteration. More importantly, in NMR T_2 measurements, the signal of crude oil often overlaps with that of bound water, making it difficult to accurately quantify pore-scale water saturation through signal integration. The use of a water–air

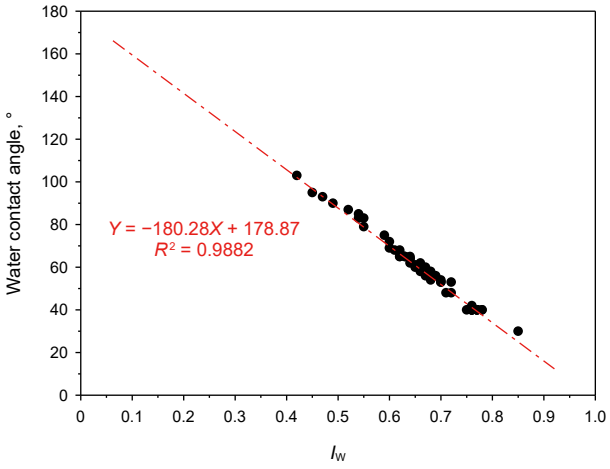


Fig. 3. Correlation between NMR-derived wettability index (I_W) and contact angle.

system effectively eliminates oil–phase signal interference, thereby improving the reliability of wettability characterization and the determination of the pore-scale water-wetness index (I_W). Therefore, the I_W index in this study is primarily engaged to evaluate the relative wettability changes of shale cores after CO_2 exposure, rather than to quantitatively simulate oil–water displacement behavior under reservoir conditions. Future studies could incorporate oil–water imbibition experiments to better represent multiphase flow processes in shale.

To further verify reliability of the pore-scale water-wetness index (I_W), water contact angles were measured to characterize macroscopic wettability of shale under the same conditions (Fig. 3). Results show that the variation trend of I_W is consistent with that of the measured contact angles. As contact angle increases, representing decrease in water-wetness, the calculated I_W value correspondingly decreases. The correlation coefficient (R^2) between I_W and contact angle is 0.9882. This consistency indicates that the NMR-based wettability index effectively captures wettability evolution of shale during CO_2 injection process.

Additionally, repeatability tests were performed through parallel experiments. The obtained NMR T_2 spectra and calculated I_W values show only minor deviations, indicating good repeatability of the proposed method. Similar NMR-based approaches have also been widely applied in reservoir characterization and fluid behavior analysis in low-permeability rocks (Dong et al., 2022).

This NMR-based wettability characterization method effectively bridges the gap between macroscopic and microscopic scales, enabling a quantitative evaluation of pore-scale wettability in complex shale reservoirs. Furthermore, by classifying T_2 relaxation times, the pore system may be subdivided into four categories: micropores, small pores, mesopores, and macropores, allowing the determination of microscopic wettability across different pore scales. By integrating T_2 spectral data under various saturation states, the core pore-scale water-wetness index (I_W) provides a robust foundation for analyzing the evolution of reservoir wettability during CO_2 injection, as discussed in the following section.

It should be noted that the pore size classification was primarily based on the distribution of NMR T_2 relaxation times. Previous studies have demonstrated that NMR T_2 is intimately related to pore size in tight and shale reservoirs and can be calibrated with conventional pore structure characterization methods such as nitrogen adsorption and mercury intrusion porosimetry (MIP) (Gao et al., 2019; Gao and Li, 2016). In general, shorter T_2 corresponds to smaller pores, whereas longer T_2 represents larger pore spaces. Based on commonly adopted classification standards in shale reservoir studies, the pore system was divided into micropores, small pores, mesopores, and macropores according to the corresponding T_2 relaxation time intervals.

3. Characteristics of shale wettability variation after CO_2 exposure

3.1. Macroscopic wettability alteration of core surface

The macroscopic wettability of core surfaces is typically characterized by water contact angle. Generally, water contact angles (θ_w) of 0°–50° correspond to strongly water-wet behavior, 50°–70° to weakly water-wet conditions, 70°–110° to intermediate wettability, and values greater than 110° correspond to oil-wet conditions (Arif et al., 2019; Cheng et al., 2021). To assess how organic precipitation influences the macroscopic wettability of shale during CO_2 injection, water contact angles were measured on core surfaces before and after CO_2 exposure under different experimental conditions (Fig. 4).

Prior to CO_2 huff-n-puff, the original cores exhibited a water contact angle of 40°, reflecting a strongly water-wet surface. In the pressure-controlled experiments, the temperature was fixed at 70 °C and the soaking period was maintained at 5 days. As the injection pressure increased, the water contact angle gradually

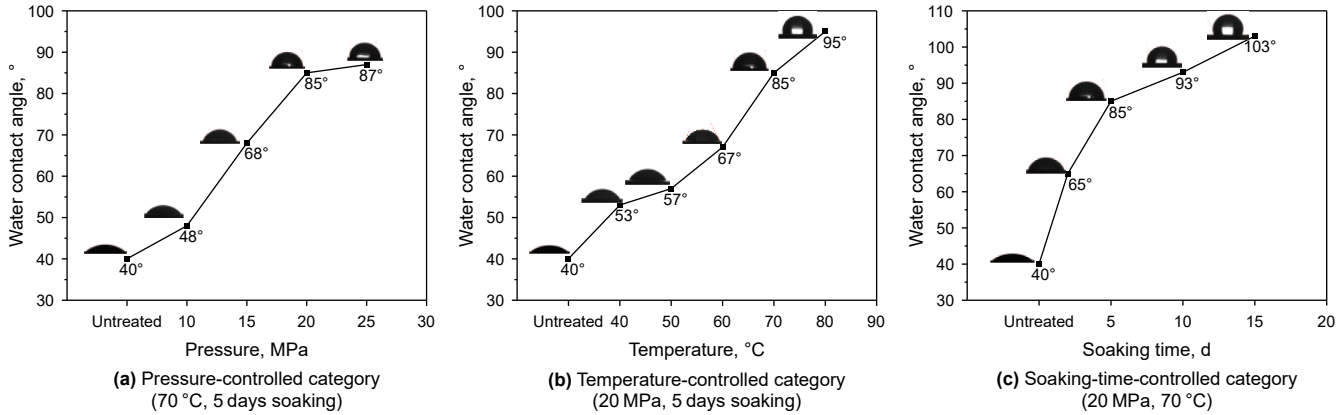


Fig. 4. Variation of macroscopic water contact angle on shale surface under different experimental conditions.

increased after CO_2 exposure, reflecting a gradual reduction in macroscopic water-wetness. Under low-pressure conditions (injection pressure <10 MPa), water contact angle rose modestly to 48°, and the core surface remained strongly water-wet. When the pressure exceeded 15 MPa, the contact angle rose sharply to 68°, indicating a transition from strong to weak water-wetness. At 20 MPa, the contact angle reached 85°, suggesting that the core surface became intermediate-wet. Further increasing the pressure to 25 MPa resulted in a contact angle of 87°, with the surface remaining intermediate-wet. In the temperature-controlled experiments, the injection pressure was fixed at 20 MPa and soaking time at 5 days. As the temperature rose, the water contact angle exhibited a gradual increase, and the macroscopic water-wetness weakened. At 40 °C, the water contact angle rose to 53° after CO_2 huff-n-puff, corresponding to a shift from strongly to weakly water-wet. As temperature rose to 80 °C, the water contact angle increased further, reaching 95°, indicating a transition to intermediate-wet state. In the soaking-time-controlled experiments, the pressure and temperature for CO_2 injection were set to 20 MPa and 70 °C, respectively. With prolonged soaking, the water contact angle rose from 40° to 103°, marking a change from strong water-wetness to intermediate-wetness. The further rise in contact angle with prolonged soaking indicates that the core surface could transition toward a weakly oil-wet state.

The reduction in water-wetness after CO_2 exposure is primarily attributed to the precipitation and adsorption of heavy organic fractions in oil, such as asphaltenes and resins, onto the core surface. Supercritical CO_2 extraction effect during injection changes the distribution of crude oil components, inducing the deposition of these heavy organics. The deposited organic layer renders the mineral surface more hydrophobic, reduces surface polarity, and ultimately shifts wettability from water-wet toward intermediate or even oil-wet. Elevated pressures and temperatures enhance CO_2 solubility and mass transfer efficiency, thereby promoting more extensive organic precipitation. Meanwhile, prolonged soaking allows additional time for the deposited organics to accumulate and adsorb on pore surfaces, resulting in more pronounced wettability alteration. Overall, the organic precipitation is the dominant mechanism responsible for macroscopic wettability changes during CO_2 injection.

Notably, the contact angle obtained in this study corresponds to the water–air–rock system rather than the water–oil–rock system, which is more representative of multiphase flow conditions in reservoirs. The water–oil–rock contact angle is directly related to capillary pressure and fluid distribution during oil–water displacement. However, due to the experimental complexity associated with measuring oil–water–rock contact angles under reservoir pressure and temperature conditions, the water–air–rock contact angle is commonly used as a proxy indicator to evaluate relative wettability changes of rock surfaces. Although the absolute values of these two contact angles may differ, previous studies have shown that their variation trends are generally consistent in reflecting wettability alteration. Therefore, the contact angle measurements are mainly engaged to characterize relative wettability changes of shale after CO_2 exposure, rather than to directly represent in-situ multiphase flow behavior.

In addition, the actual water–oil–rock system under dynamic CO_2 huff-n-puff conditions may exhibit more complex contact angle hysteresis behavior than the simplified water–air–rock system used in this study. Multiphase fluid interactions, oil redistribution, and dynamic adsorption/desorption processes during CO_2 injection may influence the evolution of contact angles under reservoir conditions. Therefore, the measured water–air–rock contact angle in this work is mainly used as a comparative indicator of relative wettability alteration. Future studies incorporating dynamic water–oil–rock contact angle measurements under reservoir conditions are recommended to further improve the understanding of wettability evolution during CO_2 huff-n-puff processes.

3.2. Microscopic pore-scale wettability alteration of cores

Based on the pore-scale water-wetness index established in Section 2.3, the pore-scale wettability evolution of shale cores after CO_2 exposure was analyzed. Fig. 5 shows the T_2 distribution of the cores before and after CO_2 injection. According to the distribution of T_2 relaxation times, the pore system is classified into four categories: micropores ($T_2 < 0.1$ ms), small pores (0.1 ms < T_2 < 1 ms), mesopores (1 ms < T_2 < 10 ms), and macropores ($T_2 > 10$ ms).

Before CO_2 injection, all dry cores exhibited a characteristic "high-left, low-right" bimodal T_2 distribution, with the left peak significantly higher. This pattern implies that abundant organic matter, structural water, and residual water in isolated pores are primarily concentrated within the micropore and small-pore regions. This observation is consistent with the 2D NMR spectra of dry cores presented in Section 3.3. After water spontaneous imbibition, the signal amplitudes across all pore-size regions increased, implying that water entered pores of various scales under capillary forces and that the cores displayed mixed-wet behavior. When the cores were subsequently saturated under high pressure, water infiltrated all connected pores, resulting in a further increase in signal amplitude. The T_2 spectra obtained at this stage represent the fully accessed pore-throat structure of shale.

After CO_2 exposure, the dried cores also exhibited the same "high-left, low-right" bimodal T_2 distribution. However. The overall NMR signal amplitude increased relative to that of the pre-reaction cores. This increase is primarily attributed to the precipitation of heavy organic components in the oil, such as resins and asphaltenes, induced by CO_2–oil interactions. Subsequently, NMR measurements were performed after spontaneous imbibition and pressurized water saturation of the reacted cores. The pore-scale water-wetness index (I_W) before and after CO_2 injection was then calculated using Eq. (1), as shown in Fig. 6. In the pressure categories, the initial I_W value of the cores before CO_2 injection was 0.77. After CO_2 exposure, I_W gradually decreased with rising pressure, indicating a progressive weakening of water-wetness. Upon reaching 25 MPa, I_W declined to 0.52. In the temperature categories, the initial I_W was 0.78 and decreased progressively with rising temperature, reaching 0.45 at 80 °C, suggesting that elevated temperatures further promote the reduction in water-wetness. In the soaking-time categories, the initial I_W was 0.76 and continued to decline with prolonged soaking, reaching 0.42 after 15 days.

The variations in the pore-scale water-wetness index before and after CO_2 exposure demonstrate that the cores became progressively less water-wet with increasing pressure, higher temperature, and longer soaking time. These trends are consistent with the macroscopic contact angle measurements, confirming the reliability of the experimental observations. Furthermore, the strong agreement between macroscopic and microscopic wettability evolution validates that the proposed pore-scale water-wetness index effectively captures and quantifies the pore-scale wettability changes.

Based on the T_2 distribution pore classification and the calculated pore-scale water-wetness index, the pore-scale wettability evolution induced by organic precipitation during CO_2 injection in shale oil cores was analyzed (Fig. 7). Under all experimental conditions, both the overall and multiple pore-scale water-wetness indices exhibited negative shifts, indicating a general reduction in water-wetness after CO_2 exposure. In the pressure-controlled experiments, higher injection pressures enhanced the extraction of

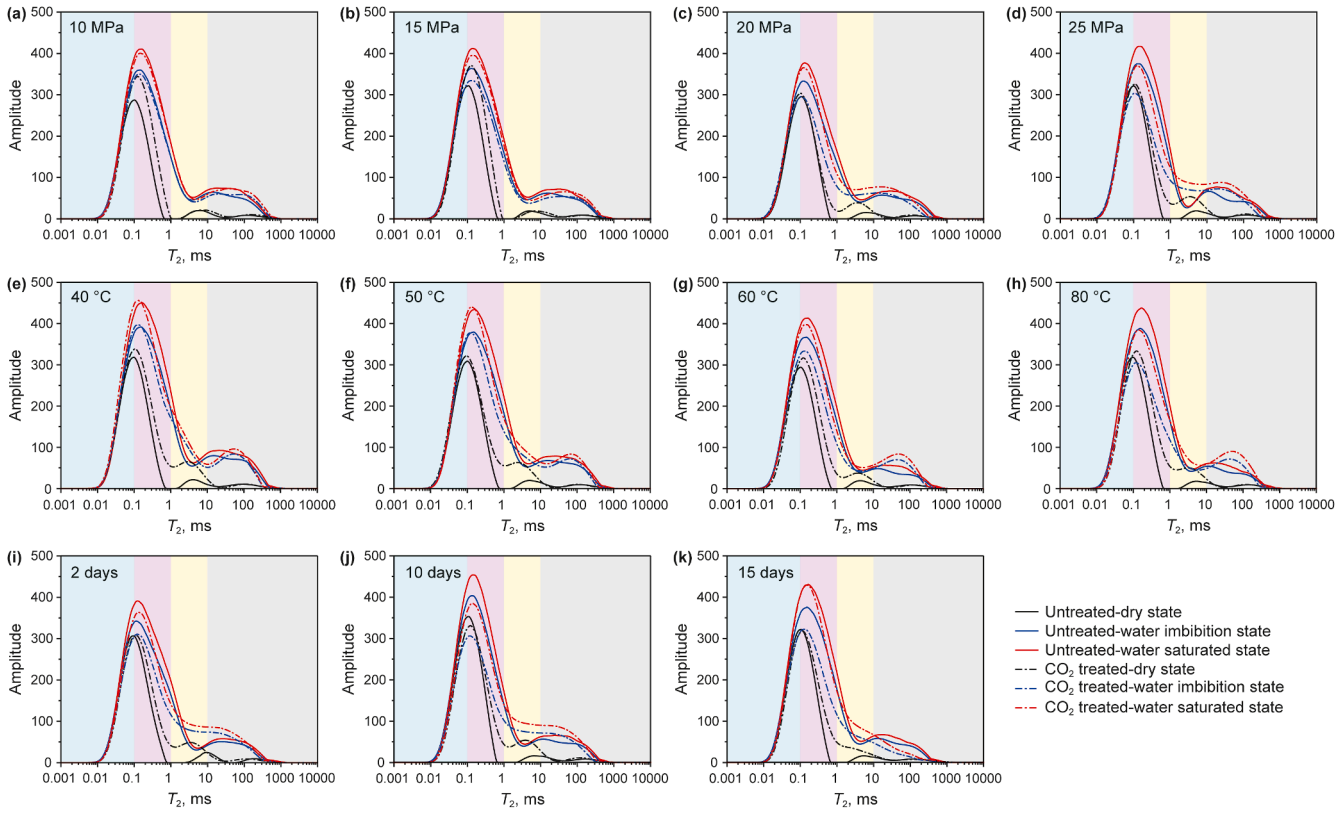


Fig. 5. Variations of NMR T_2 spectra of shale cores before and after CO_2 huff-n-puff under different experimental conditions: **(a)–(d)** different injection pressures; **(e)–(h)** different temperatures; **(i)–(k)** different soaking times.

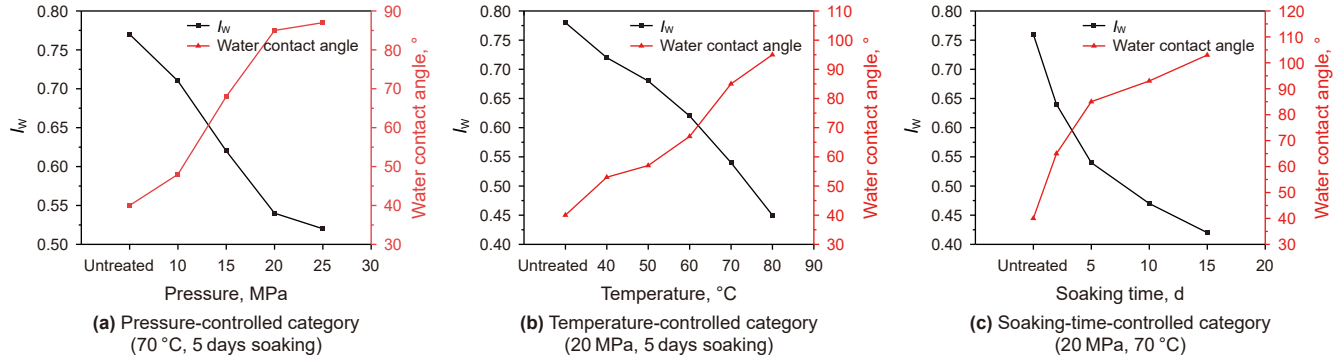


Fig. 6. Variation of core pore-scale water-wetness index (I_W) under different experimental conditions.

light and intermediate hydrocarbons from oil, thereby promoting greater precipitation of heavy organic fractions (resins and asphaltenes) and leading to a more significant decline in core water-wetness. In the temperature-controlled experiments, elevated temperatures facilitated the volatilization of light hydrocarbons and intensified CO_2–oil interactions, leading to stronger organic precipitation and a more pronounced decrease in the water-wetness index. In the soaking-time-controlled experiments, prolonged soaking enabled continuous extraction of light hydrocarbons and progressive accumulation of heavy organic precipitates, causing a gradual reduction in core water-wetness.

Moreover, the degree of wettability reduction exhibited a clear dependence on pore size. Micropores and small pores showed the most significant decreases in water-wetness, primarily because their narrow pore throats are more susceptible to surface coverage by organic precipitates. In contrast, mesopores and macropores experienced comparatively weaker changes, as their larger pore volumes and wider throats reduced the impact of organic deposition on surface wettability. Overall, the magnitude of wettability reduction followed the order: micropores > small pores > mesopores > macropores.

A correlation analysis was conducted between the water-wetness indices at different pore scales and the overall core water-wetness index under various experimental conditions after CO_2–oil–shale interactions (Fig. 8). The results indicate that wettability of small pores exhibits the strongest correlation with the overall core wettability ($R^2 = 0.9193$), followed by mesopores ($R^2 = 0.7901$), micropores ($R^2 = 0.4691$), and macropores ($R^2 = 0.4226$). The results indicate that the wettability of small pores makes a dominant contribution in governing the overall core

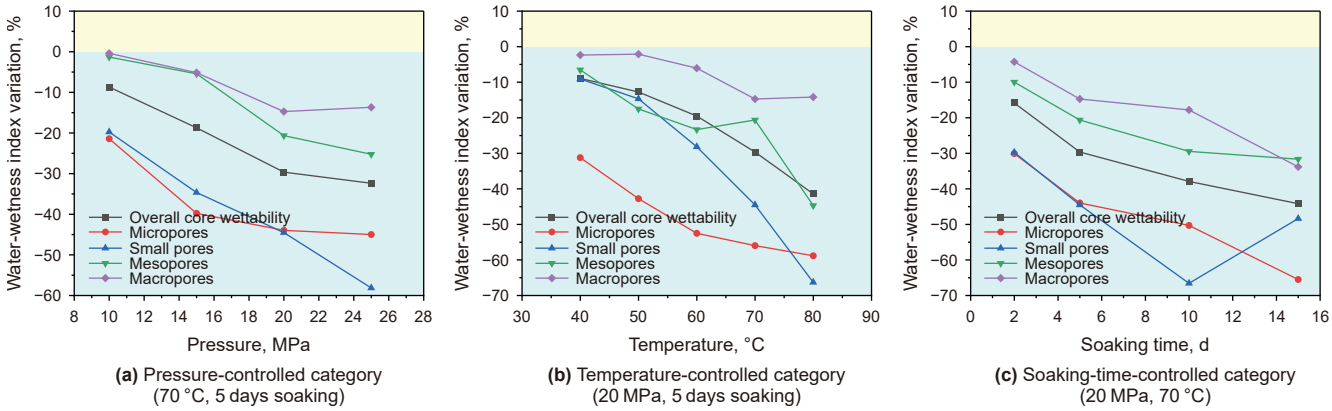


Fig. 7. Variation degree of water-wetness index in pores of different scales.

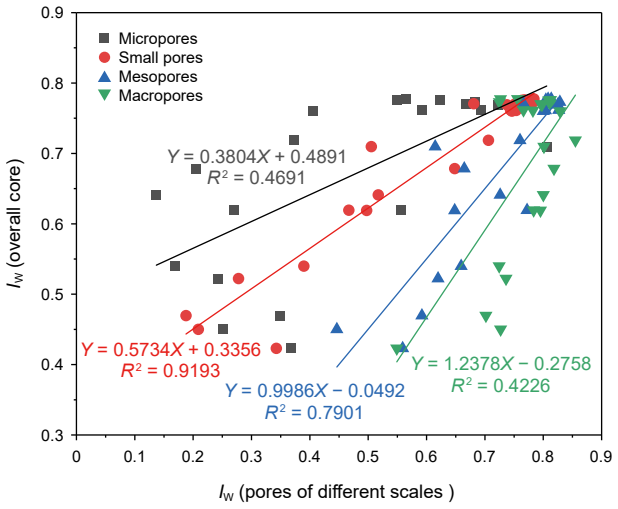


Fig. 8. Correlation between the water wetness index of pores at different scales and the overall core water wetness index after CO_2–oil–shale interactions under various experimental conditions.

wettability, primarily because small pores constitute the most abundant pore class within the pore network and thus exert the greatest influence on the core-scale wettability behavior.

3.3. Overall wettability alteration of cores

The 2D NMR T_1–T_2 spectrum provides a qualitative assessment of the overall wettability of the cores. Previous studies have demonstrated that when a fluid strongly wets the solid surface, the microscopic magnetic field gradients associated with the mineral matrix accelerate transverse relaxation, thereby shortening the T_2 relaxation time and increasing the T_1/T_2 ratio (Yan et al., 2019; Fleury and Romero-Sarmiento, 2016; Yao et al., 2024; Liang et al., 2019, 2023). Thus, comparing T_1/T_2 ratios obtained from cores saturated with a single fluid provides an effective method for assessing changes in overall core wettability. In this study, 2D NMR measurements were conducted under spontaneous imbibition conditions before and after CO_2 exposure to characterize variations in overall core water-wetness, with particular emphasis on the T_1/T_2 ratios within the capillary-bound water region of the T_1–T_2 maps. To better clarify the fluid distribution within the pore system, the T_1–T_2 spectra of the dry cores, spontaneous imbibition cores, and pressurized water-saturated cores were compared (Fig. 9).

In the dry cores (Fig. 9(a)), the signal intensity in the micropore region (T_2 < 0.1 ms) was noticeably higher than in other regions. This response primarily originates from hydrogen in organic matter and structural water bound within minerals. Previous studies indicate that T_1/T_2 ratio of organic matter is significantly higher than that of structural water, allowing signals in the T_2 < 0.1 ms region to be attributed to these two distinct components. After

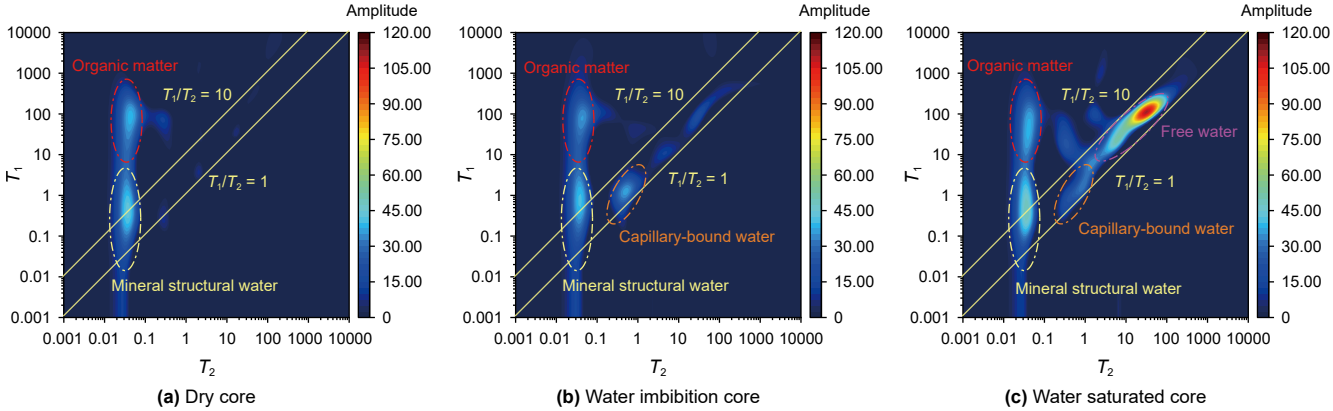


Fig. 9. Analysis of 2D NMR T_1–T_2 maps of cores under different states.

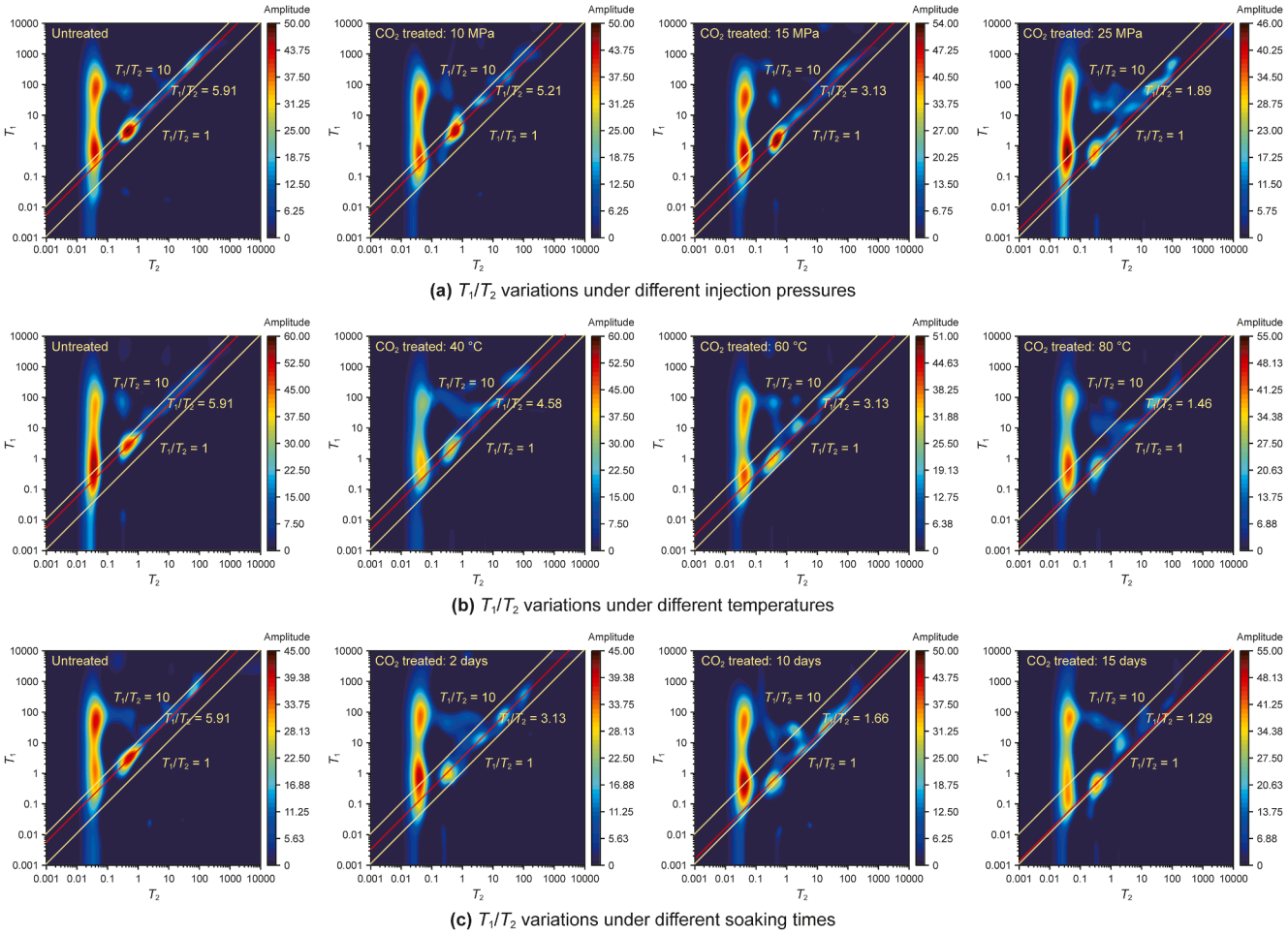


Fig. 10. 2D T_1–T_2 maps of cores under spontaneous water imbibition state before and after CO_2 huff-n-puff under different experimental conditions: **(a)** different injection pressures; **(b)** different temperatures; **(c)** different soaking times.

spontaneous imbibition (Fig. 9(b)), water entered the hydrophilic pores under capillary forces, leading to a pronounced increase in NMR signal intensity. This enhancement was most prominent in the small-pore region ($0.1 < T_2 < 1$ ms), corresponding to capillary-bound water. Following pressurized water saturation (Fig. 9(c)), the NMR signal amplitude increased markedly across all connected pores, particularly in the meso- and macropore regions ($T_2 > 1$ ms), representing free water. Since capillary-bound water primarily forms during spontaneous imbibition under capillary forces and reflects the degree of pore-scale water-wetness, overall core wettability can be assessed by analyzing the T_1/T_2 ratio within the capillary-bound water region. A higher T_1/T_2 ratio indicates stronger overall water-wetness, whereas a lower ratio corresponds to weaker water-wetness of the cores.

As shown in Figs. 10 and 11, the 2D NMR T_1–T_2 maps obtained after spontaneous water imbibition, along with the variation curves of the T_1/T_2 ratio in the capillary-bound water region before and after CO_2 exposure were analyzed to qualitatively assess the changes in overall core wettability. In the pressure-controlled experiments, the T_1/T_2 ratio in the capillary-bound water region

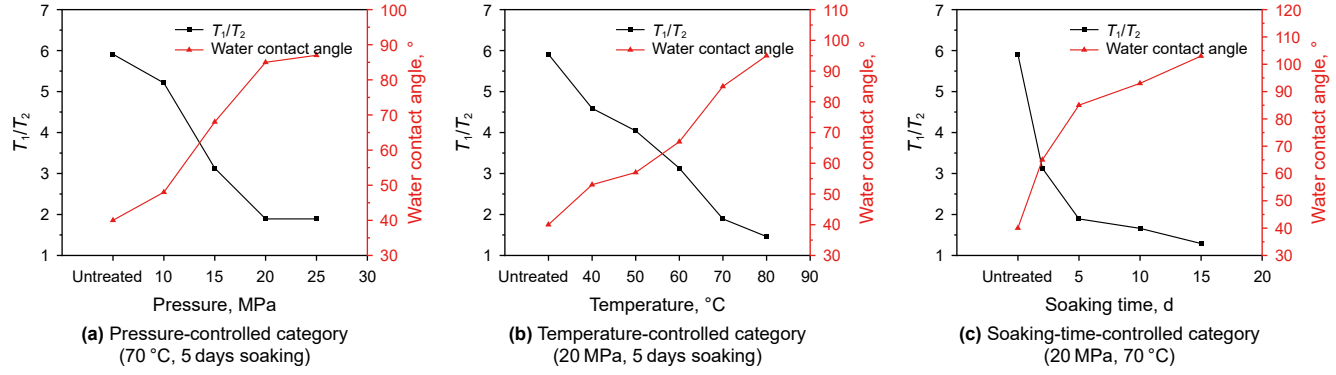


Fig. 11. Variation in the T_1/T_2 ratio of the capillary-bound water region before and after CO_2 huff-n-puff under different experimental conditions.

was 5.91 before CO_2 injection. As the huff-n-puff pressure increased, the T_1/T_2 ratio gradually decreased, indicating a reduction in overall core water-wetness. As the pressure increased to 25 MPa, the ratio declined to 1.89. In the temperature-controlled experiments, with the temperature rising from 40 °C to 80 °C, the T_1/T_2 ratio decreased from 5.91 to 1.46, suggesting that higher temperatures weakened the overall water-wetness of the core. In the soaking-time-controlled experiments, the initial T_1/T_2 ratio was 5.91 and gradually decreased to 1.29 as the soaking time increased from 2 to 15 days, indicating a progressive decline in overall water-wetness with longer soaking durations.

These observations align with the trends observed in both macroscopic water contact angle measurements and pore-scale wettability variations, confirming the reliability of the experimental results. Furthermore, they validate the T_1/T_2 ratio of the capillary-bound water region in 2D NMR maps after spontaneous imbibition serves as a robust qualitative indicator for assessing changes in overall core wettability.

It should be noted that paramagnetic minerals in the cores may influence the absolute NMR relaxation times by enhancing surface relaxation effects and local magnetic field inhomogeneity. However, all core samples analyzed were obtained from the same reservoir interval and exhibit relatively consistent mineral compositions and paramagnetic mineral contents. XRD results indicate that paramagnetic minerals are primarily pyrite and that their overall content in the selected cores is relatively low. Therefore, the influence of paramagnetic components on the relative variation trends of the T_1/T_2 ratio is considered limited. Accordingly, the T_1/T_2 ratio in this study is mainly interpreted as a comparative indicator of relative wettability evolution rather than an absolute wettability parameter.

4. Mechanisms of wettability alteration induced by organic precipitation during CO_2 huff-n-puff

4.1. Precipitation of heavy organic fractions in oil

CO_2 injection in shale oil facilitates the extraction of light and intermediate hydrocarbon fractions through CO_2–oil interactions, resulting in the accumulation of heavy organics including resins and asphaltenes. Fig. 12 presents the compositional variations of the produced oil under different experimental conditions. Prior to CO_2 injection, the original crude oil comprised 70.89% saturates, 10.40% aromatics, 13.01% resins, and 5.70% asphaltenes. After CO_2 exposure, notable compositional changes were observed. In the pressure-controlled experiments, as the pressure increased, the contents of saturates and aromatics in the produced oil gradually rose, while those of resins and asphaltenes declined. When the CO_2 injection pressure reached 25 MPa, the produced oil consisted of 82.24% saturates, 11.35% aromatics, 5.31% resins, and 1.10% asphaltenes. In the temperature-controlled experiments, increasing temperature similarly promoted higher saturate and aromatic contents and reduced resins and asphaltenes, with the produced oil at 80 °C containing 82.10% saturates, 11.83% aromatics, 5.05% resins, and 1.02% asphaltenes. In the soaking-time-controlled experiments, prolonging the soaking time led to enrichment of saturates and aromatics and a corresponding decrease in resins and asphaltenes in the produced oil. After 15 days of soaking, the produced oil consisted of 83.60% saturates, 11.51% aromatics, 3.88% resins, and 1.01% asphaltenes.

Overall, with rising pressure, elevated temperature, and prolonged soaking duration, the produced oil became progressively lighter due to the enrichment of intermediate and light hydrocarbons and the depletion of heavy fractions. These results indicate that CO_2–crude oil interactions promote the deposition of heavy organic components, which is pivotal in modifying reservoir wettability during CO_2 injection. To quantitatively evaluate the effects of resin and asphaltene deposition on reservoir wettability, the resin precipitation ratio (R_{rp}) and the asphaltene precipitation ratio (R_{ap}) during CO_2 injection were defined, as expressed in Eqs. (2) and (3), respectively.

$$R_{rp} = \frac{R_1 - R_2}{R_1} \times 100\% \tag{2}$$

where R_1 represents mass fraction of resins in the initial oil sample, %; R_2 represents mass fraction of resins in the produced oil sample, %.

$$R_{ap} = \frac{A_1 - A_2}{A_1} \times 100\% \tag{3}$$

where A_1 represents mass fraction of asphaltenes in the initial oil sample, %; A_2 represents mass fraction of asphaltenes in the produced oil sample, %.

To quantitatively evaluate the effects of resin and asphaltene deposition on reservoir wettability, correlation analyses were performed between the precipitation ratios of resins and asphaltenes and the macroscopic water contact angle of the core surface under various experimental conditions (Figs. 13 and 14). A strong positive correlation was observed between the contact angle and the precipitation ratios of resin and asphaltene. As the precipitation ratios increase, the contact angle exhibits an upward trend, signifying a reduction in water-wetness of the core surface. These findings demonstrate that the deposition of heavy organic

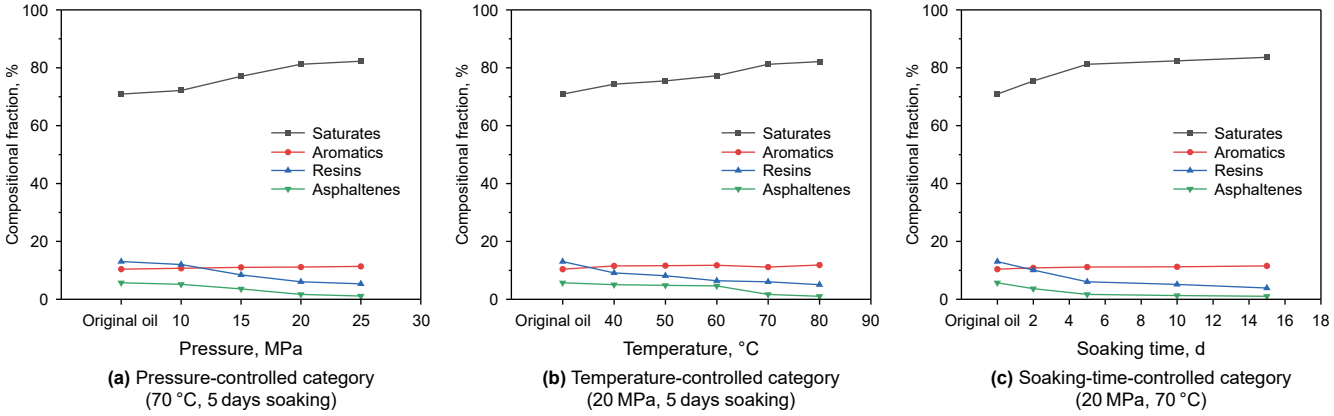


Fig. 12. Variation in produced oil composition after CO_2 huff-n-puff under different experimental conditions.

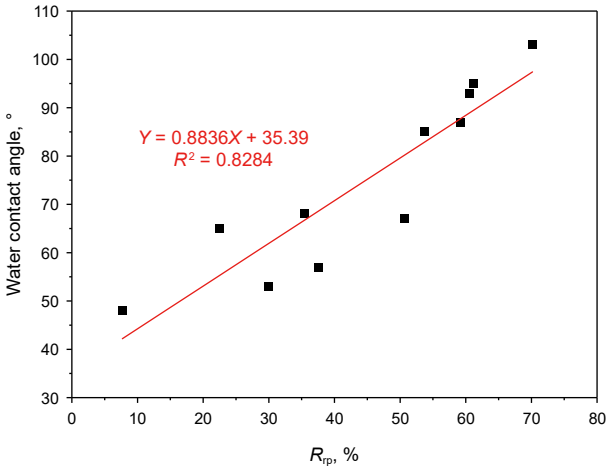


Fig. 13. Correlation between the resin precipitation ratio and the wettability contact angle.

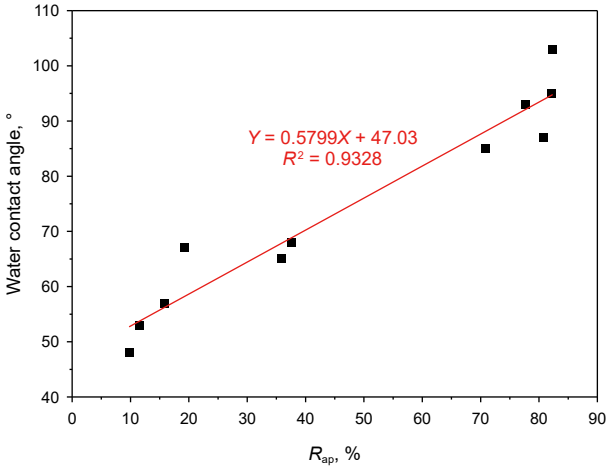


Fig. 14. Correlation between the asphaltene precipitation ratio and the wettability contact angle.

fractions, particularly resins and asphaltenes, plays a key role in modifying rock wettability during the CO_2 injection process.

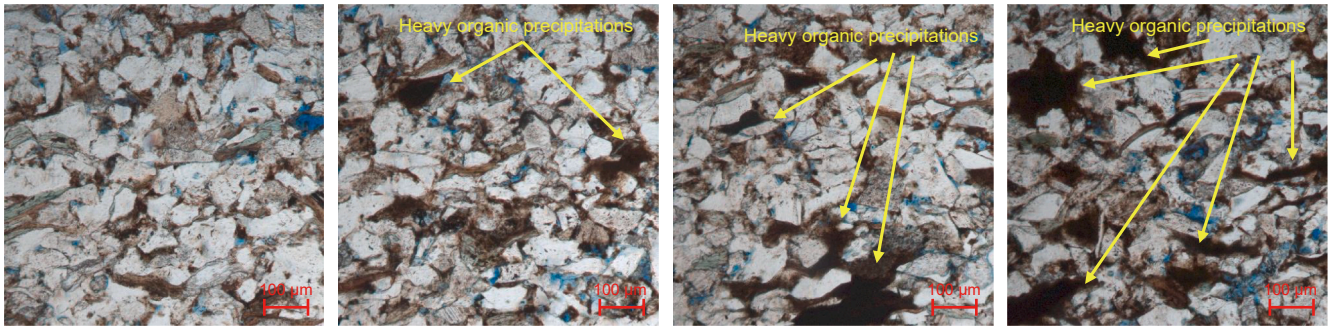
Resins and asphaltenes possess abundant polar functional groups, including phenolic hydroxyl, carboxyl, and ester groups, which can adsorb onto the rock surface through electrostatic interactions and hydrogen bonding. This adsorption process promotes the formation of a hydrophobic organic film which reduces the rock's affinity for water, resulting in a wettability transition from a strongly water-wet condition to intermediate- and oil-wet conditions. Notably, the correlation between the asphaltene precipitation ratio and the contact angle (R^2 = 0.9328) is stronger than that for resins (R^2 = 0.8284), indicating that asphaltene precipitation exerts a more pronounced effect on surface wettability alteration. This is primarily because asphaltenes have larger molecular weights, lower solubility, and more complex aromatic and polycyclic structures, which promote their precipitation and strong adsorption onto the rock surface. As a result, a relatively thick hydrophobic film forms, significantly weakening the rock's water-wetness. In contrast, resins have smaller molecular weights and weaker polarity, making them less prone to extensive precipitation and less capable of forming continuous hydrophobic films, thereby exerting a comparatively smaller influence on wettability alteration.

It should be noted that, after CO_2 treatment, the core samples in this study were depressurized to atmospheric pressure for subsequent NMR measurements and wettability characterization. In field CO_2 injection operations, however, reservoir pressure typically does not decrease to atmospheric conditions and usually remains at approximately 1000–2000 psi. Rapid depressurization to ambient pressure may reduce CO_2 dissolution in crude oil and destabilize the oil–CO_2 system, which could promote additional precipitation of heavy organic fractions such as asphaltenes.

Therefore, the extent of organic precipitation observed in laboratory experiments may be somewhat higher than that under actual reservoir conditions. Nevertheless, the experimental design allows the relative effects of CO_2 treatment on organic precipitation and wettability alteration to be systematically evaluated. Future studies could incorporate controlled pressure depletion to better simulate field pressure conditions and further quantify the pressure dependence of asphaltene precipitation during CO_2 injection.

4.2. Surface morphology alteration of the core

During CO_2 injection in shale oil, heavy organic fractions such as resins and asphaltenes precipitate from the crude oil and subsequently adsorb onto the rock surface, inducing noticeable changes in core surface morphology and significantly affecting reservoir wettability. As illustrated in Fig. 15, thin-section images of the cores captured before and after CO_2 exposure at varying pressure conditions show clear evidence of resin and asphaltene precipitation following CO_2 exposure. Furthermore, as the huff-n-puff pressure increases, both the quantity and spatial distribution of these heavy organic precipitates become more pronounced,



(a) Untreated **(b)** CO_2 huff-n-puff (10 MPa) **(c)** CO_2 huff-n-puff (15 MPa) **(d)** CO_2 huff-n-puff (25 MPa)

Fig. 15. Heavy organic deposition in core pores after CO_2 huff-n-puff under different pressures.

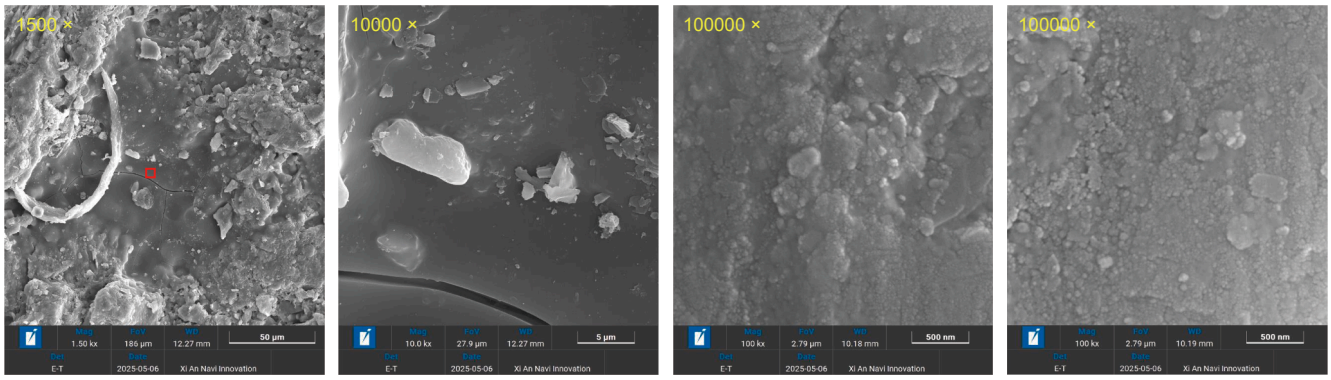


Fig. 16. SEM images of heavy fraction deposition after CO_2 exposure in shale oil.

Table 4
Relative elemental composition of the marked areas in the SEM images of heavy organic deposits (Fig. 16).

Number	Element	Relative mass fraction, %	Relative atomic fraction, %
1	C	42.50	52.38
2	O	41.46	38.32
3	N	4.87	5.14
4	K	2.24	0.85
5	Ca	8.93	3.31
Total		100	100

indicating enhanced precipitation and stronger surface coverage under higher-pressure conditions.

To further characterize the microscopic features of the precipitated heavy organics, FE-SEM coupled with EDS was employed to analyze their morphology and elemental composition. As shown in Fig. 16, FE-SEM images of the post-CO_2 exposure precipitates, together with the corresponding EDS results summarized in Table 4, reveal that the heavy organic fractions form a continuous, film-like layer on the rock surface. At a magnification of 100,000×, the precipitate displays a distinctly granular and rough surface texture. Elemental analysis demonstrates that carbon (C) is the dominant constituent, with a relative atomic fraction of 52.38%, followed by oxygen (O) at 38.32%, further confirming the organic nature of the deposited material.

The deposition of heavy organic fractions, including resins and asphaltenes, can significantly modify core surface roughness. Atomic force microscopy (AFM) was utilized to quantitatively characterize the micro- and nanoscale surface roughness of cores prior to and following CO_2 exposure and to evaluate its influence on wettability. As shown in Fig. 17, prior to CO_2 exposure, the AFM images indicate that the core surface is mainly composed of pores, throats, and microfractures, whereas the matrix displays a comparatively smooth morphology. The arithmetic mean roughness (Ra) and root-mean-square roughness (Rq) were 363 nm and 438 nm, respectively. After CO_2 exposure, the number of microscopic protrusions rose markedly, resulting in an overall enhancement in surface roughness. Both the density of surface asperities and the roughness parameters further increased with rising huff-n-puff pressures. At 25 MPa, Ra and Rq reached 455 nm and 567 nm, respectively. This roughness increase is primarily attributed to the heterogeneous deposition of resins and asphaltenes on the core surface, forming sheet-like and clustered microstructures that intensify surface undulations. These observations are consistent with the FE-SEM results, further confirming the impact of heavy organic precipitation on surface morphology.

Correlation between core roughness and water contact angle pre- and post-CO_2 huff-n-puff demonstrates that enhanced surface roughness corresponds to rising in contact angle, indicating a progressive reduction in water-wetness (Fig. 18). The contact angle exhibits strong positive correlations with both Ra and Rq, yielding correlation coefficients of 0.8942 and 0.9116, respectively. This trend is primarily attributed to the deposition of asphaltenes and resins during CO_2 huff-n-puff. These heavy organic fractions are enriched in high-molecular-weight hydrophobic hydrocarbons, which alter the chemical properties of originally hydrophilic mineral surfaces, rendering them increasingly hydrophobic. In addition, the heterogeneous deposition of resins and asphaltenes significantly increases the micro- and nanoscale roughness of the core surface. According to Wenzel's wetting model, increased surface roughness amplifies the intrinsic wettability of the surface; thus, when hydrophobic organic films form, additional roughness further enhances hydrophobicity, resulting in larger

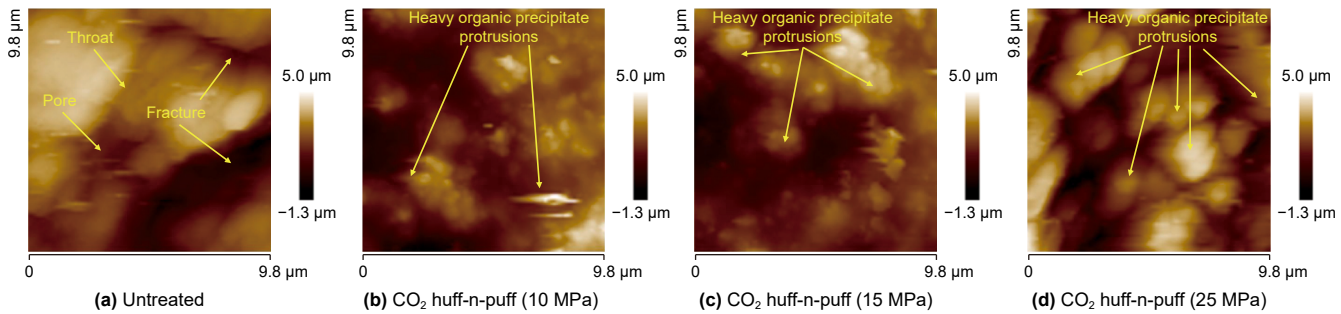


Fig. 17. AFM images of core surfaces before and after CO_2 huff-n-puff: **(a)** AFM images of untreated shale samples; **(b)** AFM images of shale samples after CO_2 huff-n-puff at 10 MPa; **(c)** AFM images of shale samples after CO_2 huff-n-puff at 15 MPa; **(d)** AFM images of shale samples after CO_2 huff-n-puff at 25 MPa.

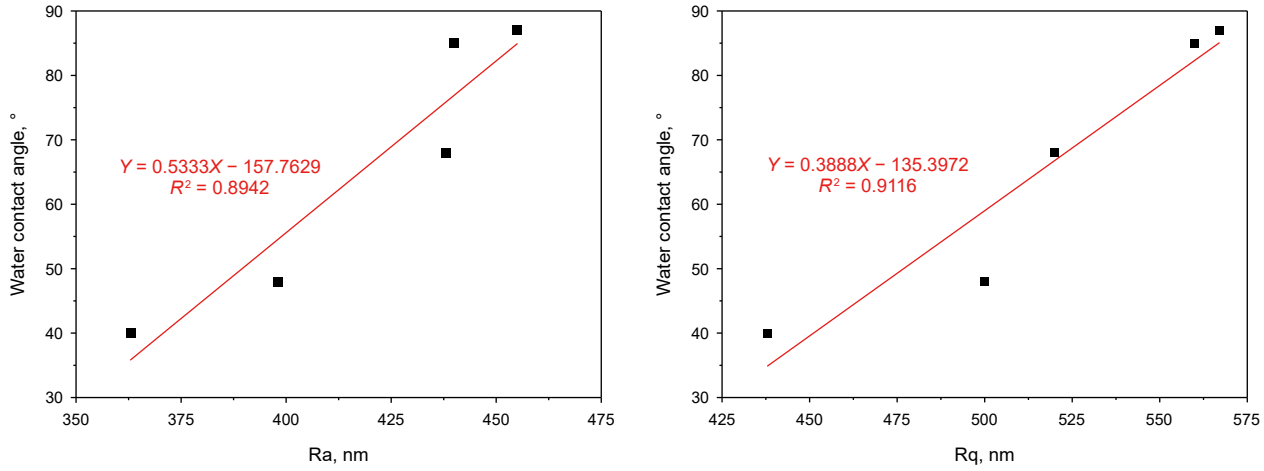


Fig. 18. Correlation between core surface roughness and water contact angle.

contact angles. Therefore, CO_2-induced precipitation of resins and asphaltenes not only modifies the surface chemistry of the core but also increases its surface roughness, and these combined effects jointly intensify the decline in water-wetness.

4.3. Pore structure evolution of the core

After CO_2 exposure, the precipitation of heavy fractions of oil reduces the effective pore volume and narrows the pore throat radius, thereby influencing the pore-scale wettability of the core. Based on the NMR T_2 spectra of pressurized water-saturated cores pre- and post- CO_2 huff-n-puff, variations in pore structure were quantitatively characterized. As depicted in Fig. 19, CO_2 huff-n-puff conducted under varying experimental conditions consistently resulting in a reduction in pore volume. In the pressure-controlled experiments, increasing the pressure from 10 MPa to 25 MPa enlarged the pore volume reduction from −2.46% to −6.94%. In the temperature-controlled experiments, elevating the temperature caused the pore volume reduction to increase from −2.04% to −8.01%. Similarly, in the soaking-time-controlled experiments, extending the soaking duration increased the pore volume reduction from −3.04% to −8.07%. This progressive decline in pore volume can be attributed to the enhanced precipitation of heavy organic fractions, with increasing pressure, elevated temperature, and prolonged soaking time. These precipitates preferentially adsorb onto the pore surfaces and partially block pore throats, forming organic coatings that reduce pore volume and diminish pore connectivity within the core.

In addition, the pore volume variation at different pore size scales was further analyzed (Fig. 20). The results show that the pore volume reduction is mainly concentrated in micropores and small pores, whereas mesopores and macropores exhibit relatively limited changes after CO_2 exposure. This behavior is attributed to the stronger confinement effect and larger specific surface area of smaller pores, which promote the adsorption and deposition of heavy organic fractions such as resins and asphaltenes. The preferential pore volume reduction in micropores and small pores is also consistent with the stronger wettability alteration observed in these pore systems in Section 3.2.

To further investigate the effect of pore structure alteration on pore-scale wettability, correlation analysis was performed between the degree of pore volume variation and the pore-scale water-wetness index after CO_2 exposure at varying experimental conditions (Fig. 21). A strong positive correlation ($R^2 = 0.9503$) is observed between these two parameters: as the pore volume variation degree becomes more negative, the pore-scale water-wetness index also decrease, indicating a progressive weakening of water-wet characteristics. This phenomenon is mainly due to the deposition of heavy organic fractions, including resins and asphaltenes, on pore surfaces during CO_2 injection. These deposits reduce the intrinsic affinity of mineral surfaces for water, shifting pore-scale wettability from water-wet toward intermediate- or

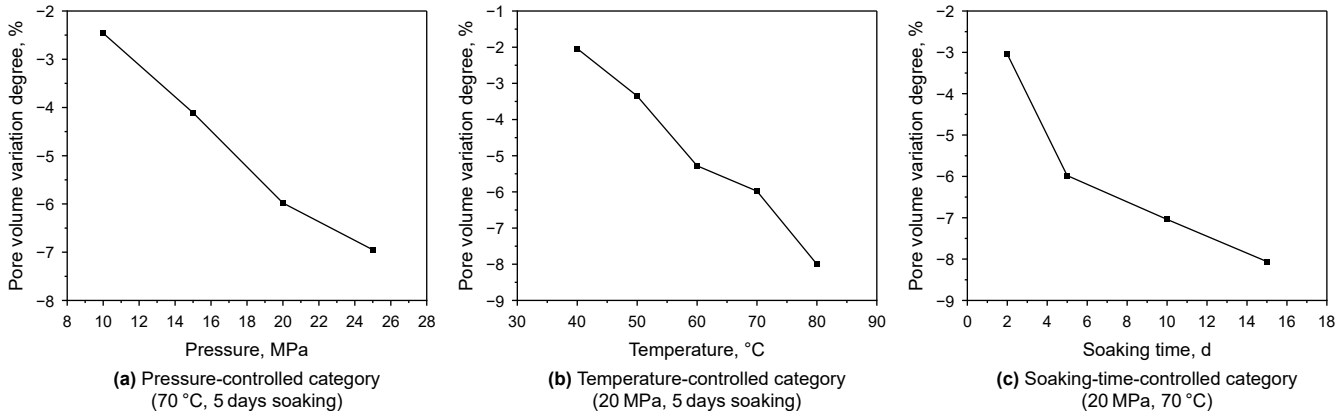


Fig. 19. Pore volume variation before and after CO_2 huff-n-puff under different experimental conditions.

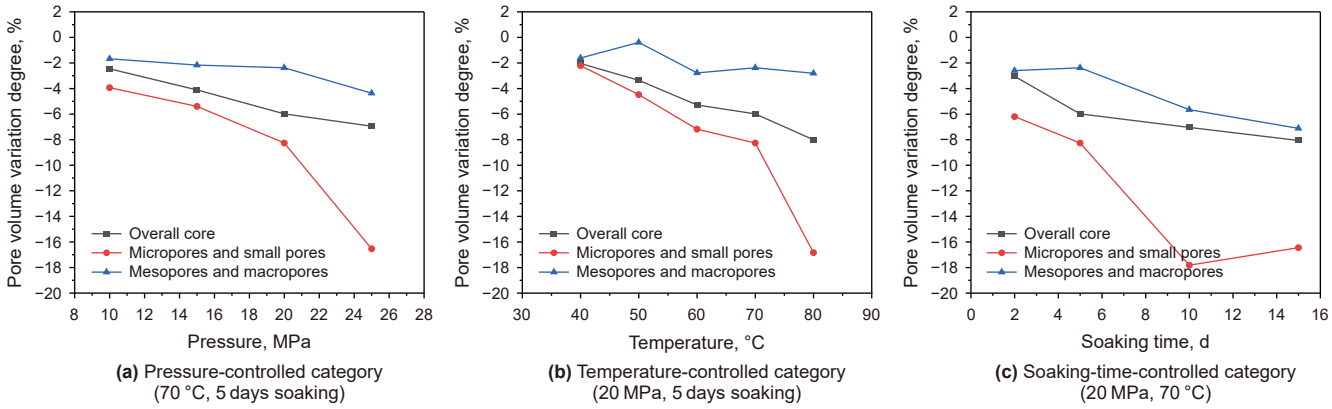


Fig. 20. Pore volume variation of pores at different scales before and after CO_2 huff-n-puff under different experimental conditions.

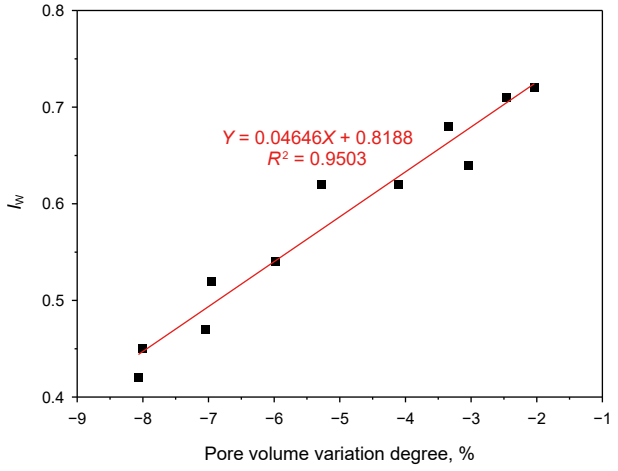


Fig. 21. Correlation between pore volume variation degree and pore-scale water-wetness index.

oil-wet conditions. During spontaneous imbibition, this wettability shift alters both the direction and magnitude of capillary forces, transforming them from promoting water entry into the pore space to resisting it. Furthermore, the reduction in pore volume and the narrowing of pore throats caused by organic deposition increase capillary pressure according to the capillary-force equation, thereby further inhibiting water intrusion. As a result, the pore-scale water-wetness index declines, and the overall water-wet behavior of shale is significantly weakened.

In addition to pore volume variation, pore surface roughness and structural heterogeneity also play important roles in controlling reservoir wettability. Fractal dimension is widely employed to describe the complexity and heterogeneity of pore structures in shale reservoirs, where higher values generally indicate increased surface roughness and heterogeneity, potentially enhancing the adsorption of heavy organic components and thereby influencing wettability alteration. Although fractal dimension was not explicitly quantified in this study, the impact of surface roughness on wettability has been quantitatively evaluated using AFM in Section 4.2. The results demonstrate that CO_2-induced organic precipitation alters the surface morphology and roughness of the core, which in turn contributes to wettability evolution. Therefore, the influence of pore surface heterogeneity has been partially captured through roughness characterization. Nevertheless, a more rigorous quantification of pore structural heterogeneity through fractal analysis, combined with NMR, nitrogen adsorption, and mercury intrusion porosimetry (MIP), is recommended for future studies to achieve a more comprehensive insight into shale pore structure and its effects on wettability.

5. Conclusions

This study investigates the Chang 7 shale oil reservoir in the Ordos Basin to elucidate the effects of CO_2-induced organic precipitation on reservoir wettability during the CO_2 huff-n-puff process. Dynamic CO_2 huff-n-puff experiments were performed in combination with contact angle measurements, 1D NMR T_2 spectra, and 2D NMR T_1–T_2 spectra. A pore-scale water-wetness index based on 1D NMR was established to quantitatively characterize microscopic wettability variations across different pore scales. By integrating analyses of oil composition, core surface morphology, and pore-structure evolution, the study reveals the mechanisms through which CO_2-induced organic precipitation alters reservoir wettability, providing valuable insights for improving recovery efficiency and evaluating the stability of geological CO_2 storage. The key conclusions can be summarized as follows.

(1) CO_2-induced organic precipitation significantly alters reservoir wettability. Increasing huff-n-puff pressure, temperature, and soaking time progressively weakens core water-wetness, shifting it from strongly water-wet to intermediate-wet, and ultimately toward weakly oil-wet conditions.

(2) Wettability alteration varies across different pore scales. The reduction in pore-scale water-wetness index follows the order: micropores > small pores > mesopores > macropores. Small pore water-wetness exhibits the strongest correlation with overall core wettability (R^2 = 0.9193), indicating its dominant contribution to overall core wettability.

(3) Asphaltene precipitation is the primary driver of wettability alteration. CO_2–crude oil interactions induce the precipitation of heavy fractions, including resins and asphaltenes, leading to a lighter produced oil. The contact angle correlates with resin precipitation at R^2 = 0.8284, and with asphaltene precipitation at R^2 = 0.9328, highlighting the stronger effect of asphaltenes on wettability.

(4) Organic precipitation alters surface roughness and pore structure, intensifying wettability alteration. Deposition of heavy organic fractions increases core surface roughness and decreases pore volume, further weakening water-wetness. The contact angle shows strong correlations with

surface roughness parameters Ra and Rq, with coefficients of 0.8942 and 0.9116, respectively, while the correlation between pore-volume variation and the pore-scale water-wetness index reaches 0.9503, indicating that pore-structure evolution plays a critical role in controlling wettability changes.

CRediT authorship contribution statement

Bo Han: Writing – original draft, Formal analysis, Data curation. **Hui Gao:** Writing – review & editing, Resources, Project administration. **Zheng-Dong Lei:** Resources, Investigation. **Kai-Qing Luo:** Resources, Investigation. **Xiao-Hang Li:** Resources, Investigation. **Guo-Qing Li:** Methodology, Data curation. **Zhi-Lin Cheng:** Resources, Investigation. **Teng Li:** Methodology, Data curation. **Chen Wang:** Formal analysis, Data curation.

Declaration of competing interest

The authors declare that they have no known competing financial interests or personal relationships that could have appeared to influence the work reported in this paper.

Acknowledgements

The authors acknowledge the financial support provided by the National Natural Science Foundation of China (No. 52474042), the Natural Science Basic Research Program of Shaanxi (No. 2025JC-JCQN-013), the National Science and Technology Major Project of China (No. 2025ZD1404804), and the Fundamental Research Program of Shanxi Province (No. 202503021212292).

References

Arif, M., Abu-Khamsin, S.A., Iglauer, S., 2019. Wettability of rock/CO_2/brine and rock/oil/CO_2-enriched-brine systems: Critical parametric analysis and future outlook. Adv. Colloid Interface Sci. 268, 91–113. https://doi.org/10.1016/j.cis.2019.03.009.

Bao, S., Ge, M., Xu, X., et al., 2023. Progress and development proposals in the exploration and development of Continental shale oil in China. Geology in China 50 (5), 1343–1354. https://doi.org/10.12029/gc20230105002 (in Chinese).

Cao, M., Gu, Y., 2013. Oil recovery mechanisms and asphaltene precipitation phenomenon in immiscible and miscible CO_2 flooding processes. Fuel 109, 157–166. https://doi.org/10.1016/j.fuel.2013.01.018.

Cheng, J., Sun, T., Wang, G., et al., 2025. CO_2 trial injection test for gulong shale oil. Pet. Geol. Oilfield Dev. Daqing 44 (6), 21–30. https://doi.org/10.19597/J.ISSN.1000-3754.202511033 (in Chinese).

Cheng, Z., Ning, Z., Kang, D.H., 2021. Lattice boltzmann simulation of water flow through rough nanopores. Chem. Eng. Sci. 236, 116329. https://doi.org/10.1016/j.ces.2020.116329.

Dong, X., Shen, L.W., Liu, X., et al., 2020. NMR characterization of a tight sand's pore structures and fluid mobility: An experimental investigation for CO_2 EOR potential. Mar. Petrol. Geol. 118, 104460. https://doi.org/10.1016/j.marpetgeo.2020.104460.

Dong, X., Shen, L.W., Liu, B., et al., 2022. Fracture's impact on the recovery of hydrocarbon from low-permeability rock's pores: New insights from 1h nuclear magnetic resonance experiment. SPE J. 27 (5), 2913–2925. https://doi.org/10.2118/209787-pa.

Dong, X.H., Xu, W.J., Liu, H.Q., et al., 2023. Molecular insight into the oil displacement mechanism of CO_2 flooding in the nanopores of shale oil reservoir. Pet. Sci. 20 (6), 3516–3529. https://doi.org/10.1016/j.petsci.2023.08.006.

Fleury, M., Romero-Sarmiento, M., 2016. Characterization of shales using T_1-T_2 NMR maps. J. Petrol. Sci. Eng. 137, 55–62. https://doi.org/10.1016/j.petrol.2015.11.006.

Gao, H., Cao, J., Wang, C., et al., 2019. Comprehensive characterization of pore and throat system for tight sandstone reservoirs and associated permeability determination method using SEM, rate-controlled mercury and high pressure mercury. J. Petrol. Sci. Eng. 174, 514–524. https://doi.org/10.1016/j.petrol.2018.11.043.

Gao, H., Li, H.A., 2016. Pore structure characterization, permeability evaluation and enhanced gas recovery techniques of tight gas sandstones. J. Nat. Gas Sci. Eng. 28, 536–547. https://doi.org/10.1016/j.jngse.2015.12.018.

Gao, H., Luo, K., Li, T., et al., 2025. Impact of CO_2 injection on mineral composition, pore structure, and mechanical properties of tight sandstone reservoirs: Implications for CO_2 geo-sequestration. Geoenergy Sci. Eng. 254, 214067. https://doi.org/10.1016/j.geoen.2025.214067.

Han, B., Cui, G., Wang, Y., et al., 2021. Effect of fracture network on water injection huff-puff for volume stimulation horizontal wells in tight oil reservoir: Field test and numerical simulation study. J. Petrol. Sci. Eng. 207, 109106. https://doi.org/10.1016/j.petrol.2021.109106.

Han, B., Gao, H., Xiao, Y., et al., 2025. CO_2 foam-assisted fracturing fluid flowback and CO_2 sequestration in tight sandstone gas reservoirs: Experimental and numerical study. Geoenergy Sci. Eng. 257 (Part A), 214199. https://doi.org/10.1016/j.geoen.2025.214199.

Huang, C., Tian, L., Wang, J., et al., 2024. Water-CO_2 wettability on sandstone surface with asphaltene adsorption: Molecular dynamics simulation. Fuel 360, 130558. https://doi.org/10.1016/j.fuel.2023.130558.

Huang, X., Tian, Z., Zuo, X., et al., 2023a. The microscopic pore crude oil production characteristics and influencing factors by DME-assisted CO_2 injection in shale oil reservoirs. Fuel 331, 125843. https://doi.org/10.1016/j.fuel.2022.125843.

Huang, X., Wang, X., He, M., et al., 2023b. The influence of CO_2 huff and puff in tight oil reservoirs on pore structure characteristics and oil production from the microscopic scale. Fuel 335, 127000. https://doi.org/10.1016/j.fuel.2022.127000.

Jia, C., Wang, Z., Jiang, L., et al., 2024. Progress and key scientific and technological problems of shale oil exploration and development in China. World Petroleum Industry 31 (4), 1–11. https://doi.org/10.20114/j.issn.1006-0030.20240530001 (in Chinese).

Jin, Z., Wang, G., Liu, G., et al., 2021. Research progress and key scientific issues of continental shale oil in China. Acta Pet. Sin. 42 (7), 821–835. https://doi.org/10.7623/syxb202107001 (in Chinese).

Lee, J.H., Jeong, M.S., Lee, K.S., 2019. Incorporation of multi-phase solubility and molecular diffusion in a geochemical evaluation of the CO_2 huff-n-puff process in liquid-rich shale reservoirs. Fuel 247, 77–86. https://doi.org/10.1016/j.fuel.2019.03.033.

Lee, J.H., Jeong, M.S., Lee, K.S., 2020. Comprehensive modeling of CO_2 Huff-n-Puff in asphaltene-damaged shale reservoir with aqueous solubility and nano-confinement. J. Ind. Eng. Chem. 90, 232–243. https://doi.org/10.1016/j.jiec.2020.07.016.

Li, B., Deng, S., Zhang, J., 2024. Producing effect of CO_2 displacement injection at high temperature and high pressure for Gulong shale oil. Pet. Geol. Oilfield Dev. Daqing 43 (1), 42–51. https://doi.org/10.19597/J.ISSN.1000-3754.202305001 (in Chinese).

Li, M., Ma, X., Jin, Z., et al., 2022. Diversity in the lithofacies assemblages of marine and lacustrine shale strata and significance for unconventional petroleum exploration in China. Oil Gas Geol. 43 (1), 1–25. https://doi.org/10.11743/ogg20220101 (in Chinese).

Li, Q., Li, Y.Y., Li, P.Y., et al., 2025. Pore structure-controlled CO_2 huff-n-puff efficiency in Jimusar shale oil reservoirs: Insights from classified oil reservoirs. Pet. Sci. 23, 2030–2045. https://doi.org/10.1016/j.petsci.2025.12.033.

Li, X., Chi, P., Guo, X., et al., 2019. CO_2-induced asphaltene deposition and wettability alteration on a pore interior surface. Fuel 254, 115595. https://doi.org/10.1016/j.fuel.2019.06.003.

Li, Z., Liu, J., Su, Y., et al., 2023a. Influences of diffusion and advection on dynamic oil-CO_2 mixing during CO_2 EOR and storage process: Experimental study and numerical modeling at pore-scales. Energy 267, 126567. https://doi.org/10.1016/j.energy.2022.126567.

Li, Z., Su, Y., Shen, F., et al., 2023b. Investigation of CO_2 storage and EOR of alternating N_2 and CO_2 injection using experiments and numerical simulation. Fuel 340, 127517. https://doi.org/10.1016/j.fuel.2023.127517.

Liang, C., Jia, Z., Xiao, L., et al., 2023. A potential NMR-based wettability index using free induction decay for rocks. Magnetic Resonance Letters 3 (3), 266–275. https://doi.org/10.1016/j.mrl.2023.03.010.

Liang, C., Xiao, L., Zhou, C., et al., 2019. Two-dimensional nuclear magnetic resonance method for wettability determination of tight sand. Magn. Reson. Imaging 56, 144–150. https://doi.org/10.1016/j.mri.2018.09.020.

Liu, B., Dong, X., Shi, X., et al., 2025a. Impacts of petrophysical heterogeneity on efficacy of CO_2 enhanced oil recovery targeting sandstones with spanning permeabilities: An experimental investigation. SPE J. 30 (10), 6211–6223. https://doi.org/10.2118/228440-pa.

Liu, J., Cao, J., Wang, J., et, 2025b. Microscopic occurrence and self-containment mechanism of continental shale oil: case study of Lucaogou Formation in Jimusaer sag, Junggar Basin. Acta Pet. Sin. 46 (7), 1355–1368. https://doi.org/10.7623/syxb202507009 (in Chinese).

Mănescu, C.B., Nuno, G., 2015. Quantitative effects of the shale oil revolution. Energy Policy 86, 855–866. https://doi.org/10.1016/j.enpol.2015.05.015.

Na, J.G., Im, C.H., Chung, S.H., et al., 2012. Effect of oil shale retorting temperature on shale oil yield and properties. Fuel 95, 131–135. https://doi.org/10.1016/j.fuel.2011.11.029.

Niu, X., Fan, J., Zhang, C., et al., 2025. Practices and research for enhanced shale oil recovery in the Qingcheng oilfield, Ordos Basin. Oil Gas Geol. 46 (5), 1664–1681. https://doi.org/10.11743/ogg20250517 (in Chinese).

Qian, K., Yang, S., Huang, F., et al., 2020. Formation damage and wettability change due to asphaltene precipitation during CO_2 injection in low-permeability reservoirs. Oilfield Chem. 37, 536–541. https://doi.org/10.19346/j.cnki.1000-4092.2020.03.028 (in Chinese).

Ren, Y.J., Wei, B., Ji, B.X., et al., 2024. Pore-scale probing CO_2 huff-n-puff in extracting shale oil from different types of pores using online T_1-T_2 nuclear magnetic resonance spectroscopy. Pet. Sci. 21 (6), 4119–4129. https://doi.org/10.1016/j.petsci.2024.07.001.

Shen, Z., Sheng, J.J., 2018. Experimental and numerical study of permeability reduction caused by asphaltene precipitation and deposition during CO_2 huff and puff injection in Eagle Ford shale. Fuel 211, 432–445. https://doi.org/10.1016/j.fuel.2017.09.047.

Tian, Y., Qu, Z., Wang, P., et al., 2023. Effect of wettability and CO_2 on asphaltene precipitation in shale oil reservoir. Energy Fuels 37 (20), 15744–15752. https://doi.org/10.1021/acs.energyfuels.3c02740.

Wang, Q., Wang, L., Glover, P.W., et al., 2020. Effect of a pore throat microstructure on miscible CO_2 soaking alternating gas flooding of tight sandstone reservoirs. Energy Fuels 34 (8), 9450–9462. https://doi.org/10.1021/acs.energyfuels.0c01431.

Wang, Q., Yang, S., Bai, J., et al., 2021. Influence of pore throat structure on changes in physical properties of reservoir rock during CO_2 flooding. Acta Pet. Sin. 42 (5), 654–668. https://doi.org/10.7623/syxb202105009 (in Chinese).

Wei, B., Zhang, X., Liu, J., et al., 2020. Supercritical CO_2-EOR in an asphaltenic tight sandstone formation and the changes of rock petrophysical properties induced by asphaltene precipitation. J. Petrol. Sci. Eng. 184, 106515. https://doi.org/10.1016/j.petrol.2019.106515.

Xu, Y., Lun, Z., Pan, Z., et al., 2022. Occurrence space and state of shale oil: A review. J. Petrol. Sci. Eng. 211, 110183. https://doi.org/10.1016/j.petrol.2022.110183.

Yan, W., Sun, J., Golsanami, N., et al., 2019. Evaluation of wettabilities and pores in tight oil reservoirs by a new experimental design. Fuel 252, 272–280. https://doi.org/10.1016/j.fuel.2019.04.130.

Yang, Y., Zhang, D., Wang, H., et al., 2025. Influencing mechanisms of solid-phase asphaltene precipitation in crude oil of Yongjin Oil Field, Junggar Basin. Petroleum Geology & Experiment 47 (4), 930–940. https://doi.org/10.11781/sysydz2025040930 (in Chinese).

Yao, H., Mei, J., Tang, J., et al., 2026. Research on integrated CO_2 huff and puff and displacement for enhanced shale oil recovery in Subei Basin. Petroleum Reservoir Evaluation and Development 16 (2), 225–237. https://doi.org/10.13809/j.cnki.cn32-1825/te.2025340 (in Chinese).

Yao, L., Yang, Z., Li, H., et al., 2024. Nuclear magnetic resonance study on wettability of shale oil reservoir. Front. Earth Sci. 12, 1287221. https://doi.org/10.3389/feart.2024.1287221.

Yuan, S., Lei, Z., Li, J., et al., 2023a. Progress in technology for the development of continental shale oil and thoughts on the development of scale benefits and strategies. Journal of China University of Petroleum (Edition of Natural Science) 47 (5), 13–24. https://doi.org/10.3969/j.issn.1673-5005.2023.05.002 (in Chinese).

Yuan, S., Lei, Z., Li, J., et al., 2023b. Key theoretical and technical issues and countermeasures for effective development of Gulong shale oil, Daqing Oilfield, NE China. Petrol. Explor. Dev. 50 (3), 562–572. https://doi.org/10.11698/PED.20230207 (in Chinese).

Yun, L., He, X., Hua, C., et al., 2023. Accumulation characteristics and resource potential of Paleogene continental shale oil in Qintong Sag of Subei Basin. Acta Pet. Sin. 44 (1), 176–187. https://doi.org/10.7623/syxb202301011 (in Chinese).

Zhao, W., Zhu, R., Liu, W., et al., 2023. Advances in theory and technology of non-marine shale oil exploration in China. Pet. Sci. Bull. 4, 373–390. https://doi.org/10.3969/j.issn.2096-1693.2023.04.029 (in Chinese).

Zhu, R., Zhang, J.Y., Li, M., et al., 2023. Advances and key issues in the basic research of non-marine shale oil enrichment. Acta Geol. Sin. 97 (9), 2874–2895. https://doi.org/10.19762/j.cnki.dizhixuebao.2023204 (in Chinese).

Zou, C., Zhu, R., Dong, D., et al., 2022. Scientific and technological progress, development strategy and policy suggestion regarding shale oil and gas. Acta Pet. Sin. 43 (12), 1675–1686. https://doi.org/10.7623/syxb202212001 (in Chinese).